Ultraviolet Laser Emission from a Micro-Pulling Down Method Grown Ce^{3+}:$LiCaAlF_6$

PHAM HONG MINH

DOCTOR OF
PHILOSOPHY

Department of Functional Molecular Science
School of Physical Science
The Graduated University for Advanced Studies

2008

Contents

Chapter 5. Conclusions and Prospects

Acknowledgements

Publications list

Chapter 1

Introduction

1.1 Introduction

The ultraviolet (UV) laser has received a great deal of interest for numerous applications in many fields of science and technology. The most established applications include environmental sensing, engine combustion diagnostics, semiconductor processing, optical micro machining, optical communications, medicine and biology [1-4]. Therefore, the improvement of laser materials or laser quality in this wavelength region is very important.

Primarily, the existing commercially available tunable UV laser sources, comprising of subsequent steps of nonlinear frequency conversion such as doubling, tripling, and/or mixing of tunable radiation obtained from traditional tunable visible or near infrared lasers have been difficult to use. The main disadvantages of such devices are their complexity, high cost, spectral bandwidth and tunability limitation in accordance with experimental requirements [5].

Recently, various new fluoride crystals have been developed as hosts to new solid-state tunable UV lasers. Cerium (Ce) doped laser materials, such as $YLiF_4$ (Ce:LYF) [6], LaF_3(Ce:LaF) [7] and more recently $LiLuF_4$ (Ce:LLF) [8,9],

$LiCaAlF_6$ (Ce:LiCAF) [10-12], $LiSrAlF_6$ (Ce:LiSAF) [13,14] crystals have been developed for use in the direct and efficient generation of tunable UV laser using a UV pump source. These have emerged as convenient and compact laser sources based on the electronically dipole-allowed interconfigurational *5d-4f* transitions of Ce^{3+} ions in wide band-gap fluoride crystals [12]. They are especially attractive for ultrashort-pulse generation and amplification in the UV region. The two most widely-used Cerium-doped crystals are Ce:LLF and Ce:LiCAF, which are tunable from 305-330 nm and 282-315 nm, respectively. In particular, Ce:LiCAF can be pumped at around 266 nm, and can be utilized as frequency-quadrupled Nd-based laser pumped sources. Ce:LLF, on the other hand, is pumped at around 250 or 289 nm. Common pump sources for Ce:LLF are frequency-doubled copper vapor lasers or KrF laser for compact systems. In addition, Ce:LiCAF or Ce:LiSAF may also be used. Moreover, Ce:LiCAF can also be used as a gain amplification medium in the UV region [15,16].

The growth method for these solid state materials has been dominated by the more popularly used Bridgman-Stokbarger [10,11] and Czochralski (CZ) methods [12,16]. To properly address the need for new or improved laser and scintillator materials, new growth schemes are proposed and even existing crystal growth techniques are modified. The micro-pulling down (μ-PD) method of crystal growth is one of the techniques developed to meet the challenges in

materials research. It can be considered as a logical continuation of the (CZ) idea of crystal pulling from the melt [17, 18]. Presently, this method is suitable only for materials survey rather than the production of highly homogeneous, high-quality crystals. There has been only one report on the successful lasing from a μ-PD method grown crystal. Lasing in the infrared (IR) region has been reported in a Nd:YAG single-crystal fiber grown by this method [19] This is the only report about lasing from a μ-PD method-grown crystal. Since the slope efficiency was a modest 22%, the μ-PD method was considered not suitable for growing high quality laser grade crystals.

In this thesis, I present experimental work on the UV lasing characteristics of a Ce:LiCAF crystal grown by a relatively new crystal growth technique, the micro-pulling down method. This work is the first demonstration of lasing in the UV region from a μ-PD method grown fluoride crystal. Chapter 2, presents an overview of previously related works on solid state UV laser materials. Background on Ce:LiCAF as a laser material is also given and the basic laser properties of this material are discussed. The μ-PD method of crystal growth is also described and compared with the classical CZ method. In chapter 3, the growth details of Ce:LiCAF by the μ-PD method is presented. A numerical calculation that was performed to help determine the optimum crystal dimensions and optical pumping parameters are described. Lastly, the

experiment set up of a laser oscillator is also discussed in detail. In chapter 4, the results and discussion are described and the important aspects of this research are summarized. Finally, chapter 5 presents the conclusion of this work. Future prospects are also outlined.

1.2 References

1. M. A. Dubinskii and P. Misra, Ultraviolet Spectroscopy and UV lasers, Marcel Dekker, Inc, (2002).
2. T. Suganuma, Hubo, O. Wakabayashi, H. Mizoguchi, K. Nakao, Y. Nabekewa, T. Togashi, S. Watanabe. Opt. Lett. **27**, (2002), 46.
3. T. Nishimatsu, N. Terakubo, H. izuseki, Y.Kawazoe, D. A. Pawlak, K. Shimamura and T. Fukuda . Jpn. J. Appl. Phys. **41,** (2002), L356.
4. R. El Ouenzerfi, S. Ono, A. Quema, M. Goto, M. sakai, N. Sarukura, T. Nishimatsu, N. Terakubo, H. Mizuseki, Y. Kawazoe, H. Sato, D. Ehrentraut, AYoshikawa and T. Fukuda . Jpn. Appl. Phys. **96**, (2004), 7655.
5. Laser Focus World, 1991, The Buyers Guide, N26.
6. DJ Ehrlich, PF Moulton, RM Osgood, Jr, Opt Lett. **4**, (1979), 184.
7. DJ Ehrlich, PF Moulton, RM Osgood, Jr, Opt Lett. **5**, (1980), 339.
8. M. A. Dubinskii, R. Y. Abdulsabirov, S. L. Korableva, A. K. Naumov, V. V. Semashko, 18 th International Quantum Electronics Conference, OSA Technical Digest. Washinton, Dc Optical Society of America, (1992), 548.
9. M. A. Dubinskii, R. Y. Abdulsabirov, S. L. Korableva, A. K. Naumov, V. V Semashko. Laser Phys. **4**, (1994), 480.
10. M. A. Dubinskii, V. V. Semashko, A. K. Naumov, R. Y. Abdulsabirov, and S. L. Korableva. OSA Proc. Adv. Solid-State Lasers. **15**, (1993), 195.
11. M. A. Dubinskii, V. V. Semashko, A. K. Naumov, R. Y. Abdulsabirov, and S. L. Korableva. Laser Phys. **3**, (1993), 216.
12. M. A. Dubinskii, V. V. Semashko, A. K. Naumov, R. Y. Abdulsabirov, S. L. Korableva. J. Mod. Opt **40**, (1993), 1.
13. J. F. Pinto, G. H Rosenblatt, L. Esterowitz, G. J. Quarles. Electron. Lett. **30**, (1994), 240.

14.C. D. Marshall, J. A. Speth; S. A. Payne; W.F. Krupke; G. J. Quarles; V. Castillo; and B. H. T. Chai, J. Opt. Soc. Am. B. **11**, (1994), 2054.

15.Z. Liu,T.Kozeki, Y. Suzuki, N. Sarukura, K. Shimamura, T. Fukuda, M. Hirano, and H. Hosono. Opt. Lett. **26**, (2001), 301.

16.D. Q. Hoa, N. D. Hung, J. Moroe, N.Takeyasu, and T. Imasaka. App. Phys. Lett. **82,** (2003), 3391.

17.K. Shimamura, N. Mujilatu, K. Nakano, S. L. Baldochi, Z. Liu, H. Ohtake, N. Sarukura, and Fukuda. J. Cryst. Growth. **197**, (1999), 896.

18.Z. Liu, S.Izumida, H. Ohtake, N. Sarukura, K. Shimamura, N. Mujilatu, S. L. Baldochi and Fukuda. Jpn. J. Appl. Phys, **37,** (1998), L1318.

19.J. Didierjean, M. Castaing, F. Balembois, and P. Georges. Opt. Lett. **31**, (2006), 3468.

20.A.Novoselov, A. Yoshikawa and T. Fukuda,Current Topics in Cryst. Growth Res. **7**, (2004), 87.

21.A. Yoshikawa, M. Nikl,G. Boulon, and T. Fukuda, Opt. Mater. **30**,(2007), 6.

22.A. Yoshikawa, T. Satonaga, K. Kamada, H. Sato, M. Nikl, N. Solovieva, and T. Fukuda. J. Cryst. Growth **270**, (2004), 427.

Chapter 2

Background and Previous Works

2.1 Review on Ce-doped Fluoride crystals

Since 1979, Ce^{3+} activated dielectric crystal are the most attractive candidates for the applications as UV tunable solid-state laser media [1]. Cerium (Ce) doped $LiYF_4$, LaF_3, $LiLuF_4$, $LiCaAlF_6$, and $LiSrAlF_4$ crystals have been developed for use in the direct and efficient generation of a tunable UV laser using a UV pump source[1-8].

Figure. 2.1 shows the energy level structure of Ce^{3+} when doped into a fluoride host. In the lattice, the outer 5s and 5p closed shells shield the 4f level from the crystal field. In this case, the weak field treatment of the crystal field interaction leads to Stark splitting of the $F_{7/2}$ and $F_{5/2}$ manifolds, with typical Stark level splitting of 100 cm^{-1}. Conversely, due to the large spatial extent of the 5d wavefunction, beyond the 5s and 5p orbitals, the crystal field interaction dominates over the spin orbit interaction, depressing and splitting the 5d configuration into a number (typically 4 or 5) of broad Stark levels, each separated by 5 000 cm^{-1}. The first excited configuration of the Ce^{3+} free ion, formed by promotion of the 4f electron to the 5d energy level, is also split by the spin orbit interaction into the $^2D_{3/2}$ and the $^2D_{5/2}$ energy levels which lie at 49 737 and 52 226 cm^{-1}, respectively. The number and position of the Stark levels are dependent on symmetry and the strength of the crystal field [9, 10, 11].

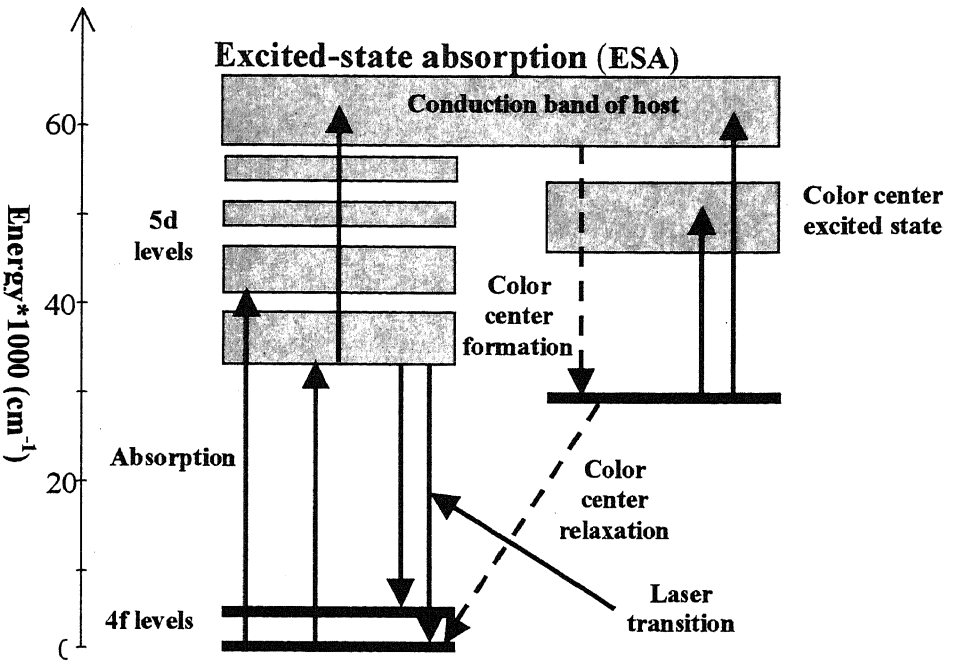

Fig. 2.1. **The energy level structure for trivalent cerium ion in a fluoride host.**

UV lasing occurs due to the 5d → 4f transition, in contrast to the IR 4f → 4f transition commonly employed in other trivalent lanthanide laser schemes such as Nd:YAG. While transitions within the 4f manifold are only permitted by mixing of opposite parity orbitals into 4f states by odd crystal field components, the 5d → 4f transitions in rare earth ions are electric dipole allowed. Thus, the 5d → 4f transitions have far higher electric dipole matrix elements and correspondingly smaller radiative lifetimes (a few tens of nanoseconds versus hundreds of microseconds) than the familiar IR transitions. Due to the large energy gap between the Ce laser levels (typically 20 000 to 30 000 cm^{-1}), the probability of multi-phonon related nonradiative decay is low [12], resulting in high (90%) quantum efficiencies [5, 11].

In some hosts, transitions involving higher lying excited states of the cerium ion, the conduction band, and color centers may all play important roles

in the UV spectroscopy [13]. The 5d → conduction band ESA transition and a color center formation mechanism, which is important for some of the Ce^{3+}-doped fluorides, are shown in Figure. 2.1. Color centers may form when an electron, promoted to the conduction band following an ESA event, is trapped at a lattice defect or impurity site. Color center lifetimes vary with impurity trap depths, and with temperature, as they are thermally deactivateable. The color centers have a deleterious effect on the lasing characteristics because color centers can potentially absorb at pump or laser wavelengths, leading to solarization, which in turn cause losses. Such absorption may promote the trapped electron to bound states of the trap or promote the electron back to the conduction band, whereupon the electron may return to a Ce^{3+} site, removing the color center.

The laser operation is based on the electrically dipole-allowed interconfigurational *5d*-*4f* transitions of Ce^{3+} ions in the host crystal. Because of the strong lattice interaction with *5d* electrons, the fluorescence that results from *5d*-*4f* transitions of trivalent rare-earth ions in solid hosts is characterized by its broad bandwidth and large Stokes shift. Such fluorescence is particularly attractive for the development of UV lasers. The most important characteristics of such a crystal is its broad gain bandwidth arising from the transition of two orbit-spin doublet levels of $^2F_{5/2}$ and $^2F_{7/2}$, separated by 2 253 cm^{-1} in the *4f* configuration [1, 9]. Depending on the crystal host, strong crystal-field splitting of the 5d levels leads to four or five broad absorption bands, the lower laser level being the 4f level ($^2F_{5/2}$ and $^2F_{7/2}$).

Their most noteworthy attribute is that direct lasing can be achieved with pumping by the higher order harmonic of a Nd:YAG laser. In particular, Ce:LiCAF and Ce:LiSAF can be pumped by the fourth harmonics and Ce:LLF and Ce:YLF can be pumped by the fifth harmonics. Among these crystals,

Ce:LiCAF proved to have sustained high output due to the absence of solarization effects [8], following its invention and initial lasing as reported by Dubinskii et. al.

Ever since these new Ce-doped crystals were reported, studies on the solid-state ultraviolet tunable lasers have become popular again. All these new Ce-doped crystals have a broad gain-bandwidth in the ultraviolet region, which is especially attractive for ultrashort pulse generation and amplification. The tunable wavelength regions of the five known Ce-doped laser crystals are shown in Figure. 2.2.

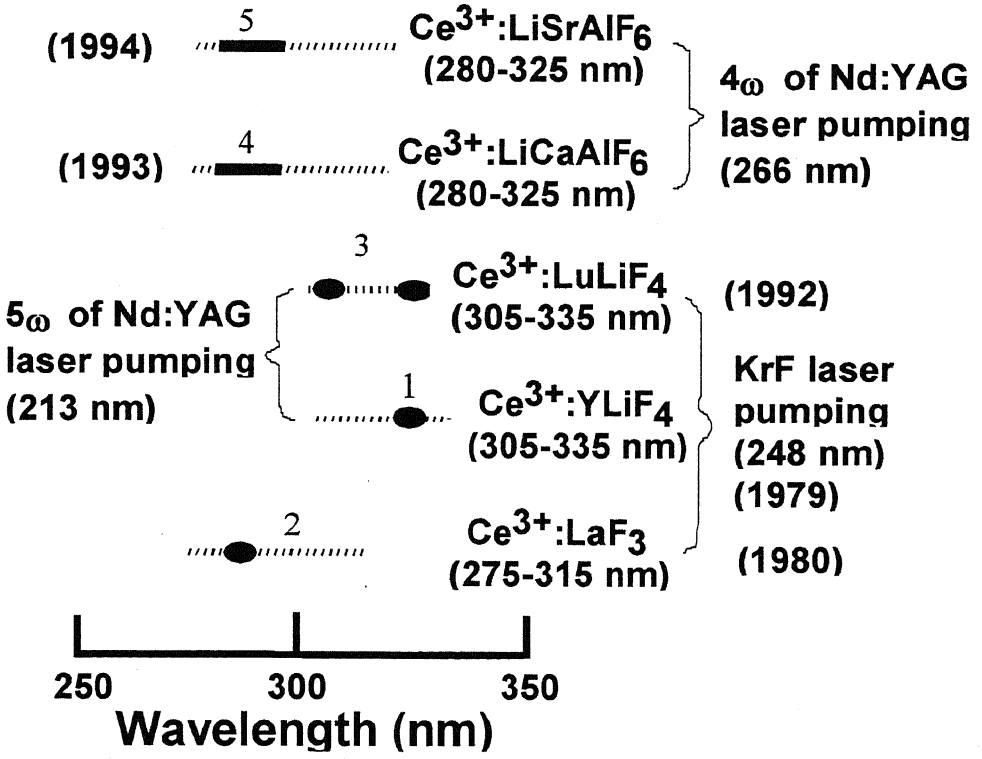

Fig. 2.2. **Various tunable lasers in ultraviolet region. Solid lines and dots indicate the confirmed tunable wavelength region, dotted lines show potential tunable wavelength region.**

2.2 Basic properties of a Ce:LiCAF laser medium

The first report for Ce:LiCAF is given by Dubinskii, et al. in 1993, which can be pumped by fourth harmonic of a Nd:YAG laser. Remarkably, no solarization effect was observed from this crystal [6-8]. The Ce:LiCAF fluorescence and absorption spectra, shown in Figure. 2.3, displays the nearly two-hump shaped characteristic of Ce^{3+} ions in most known hosts due to the allowed $5d$-$4f$ transitions terminating at the $^2F_{5/2}$ and $^2F_{7/2}$ components of the spin-orbit split ground levels. The maximum absorption is found at about 200 nm but a strong absorption also appear at 266 nm (a). The excitation wavelength at 266 nm is also indicated in the Figure.

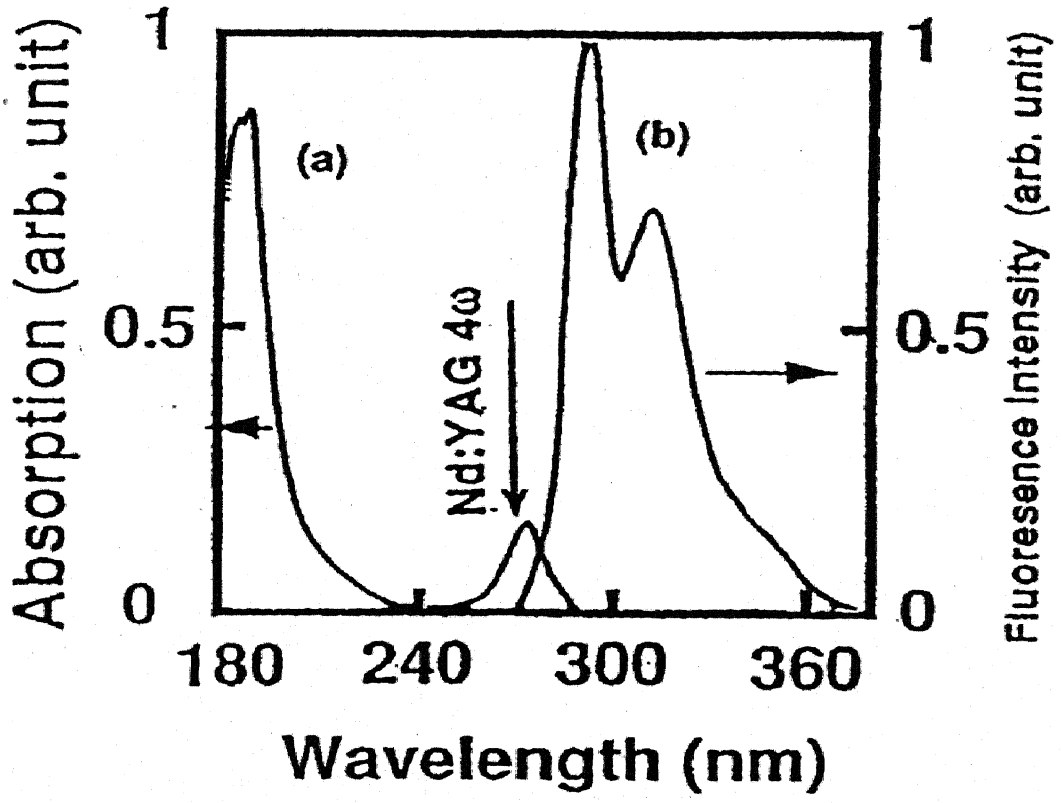

***Fig. 2.3*. The absorption and fluorescence spectra of a Ce:LiCAF crystal [5,6] (a) Absorption spectrum, (b) fluorescence spectrum**

The main advantages of Ce:LiCAF are shown below.

- Because Ce:LiCAF has a strong absorption at 266 nm, the fourth harmonic (4^{th} harmonic) of the Nd:YAG laser is an ideal pump source.
- Ce:LiCAF has a potential tuning range from 280 to 320 nm [7]. This tuning range is attractive for short pulse applications.
- Ce:LiCAF has a sufficiently higher effective gain cross-section ($6x10^{-18}$ cm^2) compared with Ti:sapphire [14]. This property makes it favorable for designing laser oscillators.
- Ce:LiCAF has a larger saturation fluence (115 mJ/cm^2) than organic dyes [8]. This makes it attractive for designing power amplifiers.
- The fluorescence lifetime of Ce:LiCAF was reported to be 30 ns and is shown in Figure. 2.4 [15]. This lifetime is shorter than that of Ti:sapphire. Although it is too short for constructing regenerative amplifiers, it is long enough for designing multipass amplifiers and also long enough for electric delay control of the amplifier timing.

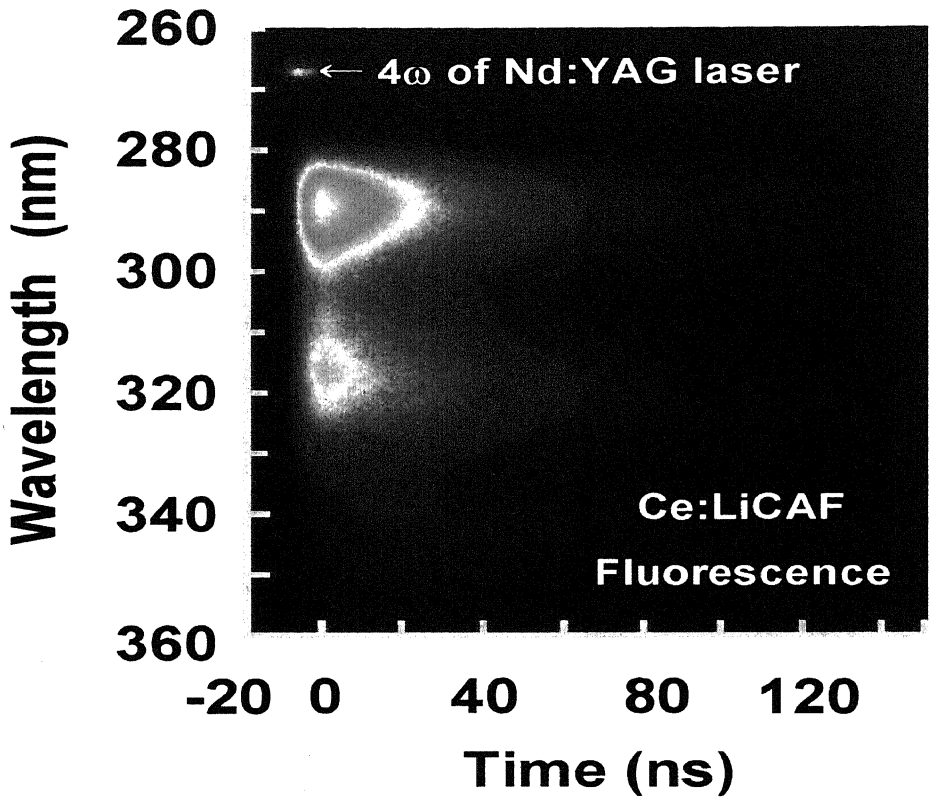

Fig. 2.4. **Streak camera image of florescence of Ce:LiCAF excited by 4th harmonic of Nd:YAG [15].**

2.3 Crystal growth methods

Part of the difficulty in developing new materials is the high cost and difficulty in producing large crystals by standard crystal growth methods. This is very important for many industrial applications such as fabrication of electrical and optical devices. To efficiently address the need for suitable materials, the μ-PD method modified for fluoride crystal growth is used.

Over the last decade, the μ-PD method was proposed by Dr.Ohnishi at the Electro Technical Laboratory in Tsukuba Japan. It was later established at the Fukuda Laboratory, at the Institute of Material Research, Tohoku University in Sendai, Japan. This new method is relatively simple and it could be considered as a logical continuation of classical methods of crystal pulling from the melt [16]. It can be categorized as a shaped crystal growth method because of its capability of growing crystals of different shapes such as fibers, rods, and tubes. The schematic diagram for the initial resistively heated μ-PD apparatus is shown in Figure. 2.5. Raw material is placed in a crucible made of metal, for instance Pt or Pt/Rh that is stable at a high temperature corresponding to the melting point of the crystalline material to be grown. The crucible has a micro nozzle with a capillary at the bottom. The temperature of the nozzle can be controlled to a high degree of accuracy by the power load to the Pt-wire after heater. The weight of crucible charge is less than 1 gram and additional feeding can be provided during the growth process. The crucible is resistively heated directly. After it has reached the material's melting point, a thin seed crystal is touched to the hanging melt droplet at the nozzle. The fiber is then pulled down with a speed of 0.01-20 mm/min. Alignment of the seed and the nozzle is controlled by a micro X-Y stage. Growth is usually conducted in air atmosphere. The crystal diameter can

be controlled from 0.115-2 mm by using an after-heater. An optical microscope enables visual monitoring of the growth process. This provides excellent conditions for in situ observation of the growth interface through a fully transparent meniscus.

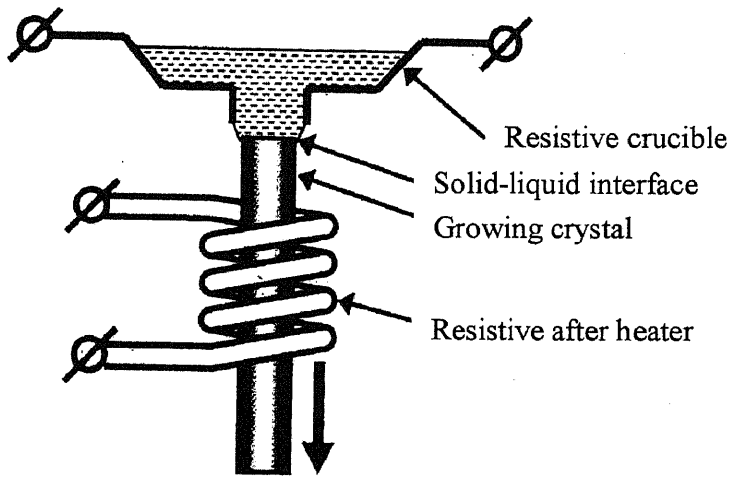

***Fig. 2.5*. Schematic diagram of the resistively heated micro-PD apparatus [18].**

Several works on the successful growth of oxide crystals have demonstrated the advantages of this method. From these, the following features of the μ-PD method were established [19-24].

- Owing to a fast growth speed, a high quality single crystal can be grown from less than 1 g of raw material in 5-12 hours, thereby allowing growth of large crystals at a shorter time and at a lower cost compared with other melt growth methods like CZ or Bridgman. This very high growth speed makes the μ-PD method a unique tool for single crystalline material screening.

• Moreover, this method has the capability of controlling the shape of a grown crystal, for example, fibers, rods, and tubes because the crucible not only serves as a container for the melt but also as a shaper for shaped crystal growth.

• Repeated seeding can be utilized to produce a few crystals of similar length without cooling the hot zone to room temperature. The design of the μ-PD machine allows sealing failure for 5-10 min without oxidation of the Ir crucible. The as-grown crystal is cut and removed, then the system is sealed again and the seeding procedure is repeated. The number of crystals grown is therefore limited by the crucible charge.

• Lower thermal distortion decreases the density of dislocation or cracks.

• The use of narrow nozzle suppresses melt convection. For fast pulling rates this leads to the effective segregation coefficient near unity and allows growth even from an incongruent melt composition.

• It is easy to control the crystal diameter or shape by minor change of the nozzle capillary.

A comparison between the Czochralski and the Micro-Pulling down methods are summarized in Table 1.

Characteristics	Cz	Micro-PD
Growth direction	Upward	Downward
Typical Growth rate	0.05 – 0.1 mm/h	0.05-1 mm/min
Amount of raw material	Plenty	< 1 g
Maximum crystal diameter	400 mm	0.05 - 10 mm
Maximum crystal length	1-2 m	1 m
Stage of development	Grow crystals for actual devices	Research stage for materials screening
Other characteristics	Large crystals, less inclusion of heavy solid particles	Shaped crystal growth, "ready to use" fibers, multi-crystal growth, less inclusion of air bubbles

Table 2.1 **Comparison between the Cz and the μ-PD method**

Considering these applications, the innovation of the μ-PD apparatus to accommodate fluoride crystal growth was carried out. Moreover, extensive research was put into the improvement of this method to facilitate the screening of fluoride host lattices, dopant concentration and optimization of the growth parameters. The concept is similar with the previously discussed μ-PD growth schemes and will be discussed more in the next chapter.

2.4 References

1. D. J. Ehrirlich, P. F. Moulton, and R. M. Osgood, Jr. Opt, Lett. **4** (1979), 185
2. DJ Ehrlich, PF Moulton, RM Osgood, Jr. Opt Lett. **5**, (1980), 339.
3. MA Dubinskii, RY Abdulsabirov, SL Korableva, AK Naumov, VV Semashko, 18 th International Quantum Electronics Conference, OSA Technical Digest. Washinton, Dc Optical Society of America. (1992), 548.
4. MA Dubinskii, RY Abdulsabirov, SL Korableva, AK Naumov, VV Semashko. Laser Phys. **4**, (1994), 480.
5. M.A. Dubinskii, V.V. Semashko, A.K. Naumov, R.Y. Abdulsabirov, and S.L. Korableva. OSA Proc. Adv. Solid-State Lasers **15**, (1993), 195.
6. M.A. Dubinskii, V.V. Semashko, A.K. Naumov, R.Y. Abdulsabirov, and S.L. Korableva. Laser Phys. **3**, (1993), 216.
7. M. A. Dubinskii, V.V. Semashko, A. K. Naumov, R.Y. Abdulsabirov, S. L. Korableva. J. Mod. Opt. **40**, (1993), 1.
8. C.D. Marshall, J.A. Speth; S.A. Payne; W.F. Krupke; G.J. Quarles; V. Castillo; and B.H.T. Chai, J. Opt. Soc. Am. B. **11**, (1994), 2054.
9. R. J. Lang, "The spectrum of trebly ionized cerium," Can. J. Res. A. **14**, (1936) 127-130.
10. B. Henderson and R. H. Bartram, Crystal-Field Engineering of Solid State Laser materials. Cambridge, U.K: Cambridge Univ. Press, (2000)).
11. P. Dorenbos. Phys. Rev. B. **62**, (2000), 15640.
12. M. J. Weber, Solid State Commun., **12**, (1973), 741.
13. M. F. Joubert, Y. Guyot, B. Jacquier, J. P. Chaminade, and A. Garcia. J. Fluorine Chem. **107**, (2001), 235.
14. PF Moulton. J. Opt.Soc. Am. B. **3**, (1986), 125.

15. T.Kozeki, Y. Suzuki, M. Sakai, H. Ohtake, N. Sarukura, K. Shimamura, T. Fukuda, T. Nakajyo, F. Sakai, and Y. Aoki. Appl. Phys. B. **74**, (2002), S185.
16. T. Fukuda and V. Chani. Springer, Germany, 2007.
17. A. Novoselov, A. Yoshikawa and T. Fukuda. Current Topics in Cryst. Growth Res. **7**, (2004), 87.
18. A. Yoshikawa, M. Nikl,G. Boulon, and T. Fukuda, Opt. Mater. **30**, (2007), 6.
19. B. M. Epelbaum, K. Inaba, S. Uda, and Fukuda, J. Cryst. Growth, **178**, (1997), 426.
20. B. M. Epelbaum, K. Inaba, S. Uda, K. Shimamura, M. Imaeda, V. V. Kochurikhin, and T. Fukuda. J. Cryst. Growth. **179** (1997), 559.
21. D. H. Yoon, I. Yonenaga, T. Fukuda, N. Ohnishi. J. Cryst. Growth. **142** (1994), 339.
22. Fiber Crystal Growth from the Melt, T. Fukuda, P. Rudolph, S. Uda, (Eds), Springger, Berlin. (2004).
23. A. Yoshikawa, T. Satonaga, K. Kamada, H. Sato, M. Nikl, N. Solovieva, and T. Fukuda. J. Cryst. Growth. **270**, (2004), 427.
24. A. Yoshikawa, K. Kamada, M. Nikl, K. Aoki, H. Sato, J. Pejchal, and T. Fukuda. J. Cryst. Growth. **285**, (2005), 445.

Chapter 3

Numerical Simulation and Experiment

3.1 Numerical Simulation

The crystal sample that was studied is relatively new, thus, its basic optical properties have to be investigated. Primarily, given specified experimental parameters I wanted to determine the important optical parameters of the Ce:LiCAF sample, in order to design the appropriate experimental conditions. For this purpose, numerical simulations were carried out using the Matlab software, where pertinent equations and parameters are programmed. The software then carries out the mathematical calculations based on the algorithm. The properties that were investigated using numerical methods were radius, absorption coefficient, and absorption profile for specified given values of optical pump beam diameter, pump energy and an assumed refractive index for Ce:LiCAF. I considered a cylindrical Ce:LiCAF crystal that was optically excited by a collimated beam in a side pumping scheme as shown in Figure. 3.1. The beam diameter was made to be equal to the sample diameter in all the calculations while keeping the power constant at 100 mJ.

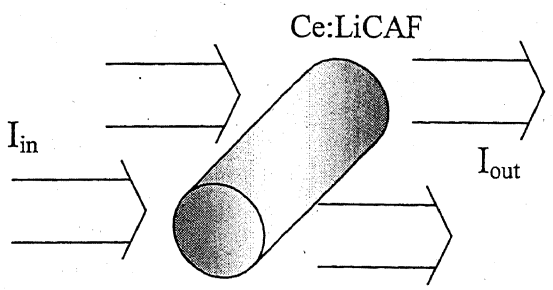

Fig. 3.1. **The crystal was optically excited by a collimated beam in a side pumping scheme.**

In Figure. 3.2, I show the cross section of the optical setup, having a specified crystal refractive index of 1.4. The light rays of the optical excitation will be refracted as shown, according to Snell's Law given by the equation (3.1), [1].

$$\frac{\sin\ \theta_1}{\sin\ \theta_2} = \frac{n_2}{n_1} \quad , \tag{3.1}$$

where n_1 is the refractive index of air, n_2 is that of Ce:LiCAF, (n_2=1.4), θ_1 is incident angle and θ_2 is the refraction angle inside the crystal.

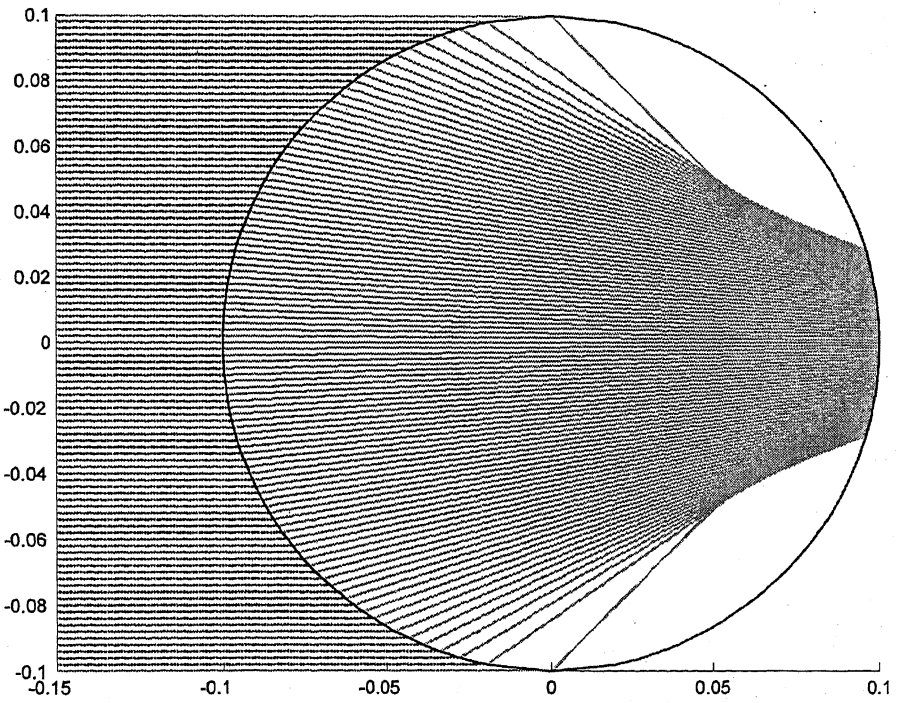

Fig. 3.2. **The cross section of the crystal showing the refracted rays in a side-pumping scheme. The electric field distribution inside the crystal is not uniform.**

The cross section clearly demonstrates that there will be regions inside the crystal where the refracted light rays will intersect, therefore, the electromagnetic field distribution inside the sample is not uniform. These results were used to numerically determine the optical absorption profile

inside the cylindrical crystal for side pumping geometry. Using Beer-Lambert's equation (3.2), [2].

$$I = I_0 \exp(-\alpha l) \tag{3.2}$$

where I is the intensity after passing through the material, I_0 is the intensity of the incident light, l is the lateral distance in the sample, and α is absorption coefficient of the material.

Moreover, using Beer-Lambert's equation again, I studied the dependence of the absorption ratio, η, on the crystal radius and absorption coefficient defined by.

$$I_{abs} = I_{pump}[1 - \exp(-\alpha l)] \tag{3.3}$$

$$\eta = \frac{I_{abs}}{I_{pump}} \tag{3.4}$$

$$\eta = 1 - \exp(-\alpha l) \tag{3.5}$$

I also calculated absorption profile for two-side pumping as shown in Figure. 3.3.

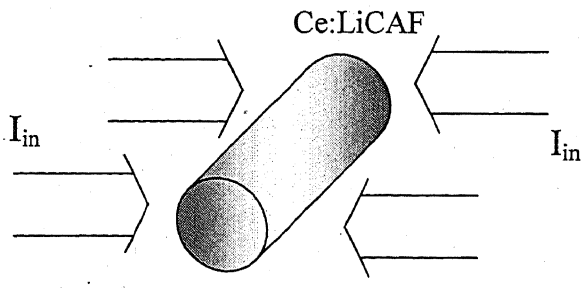

Fig. 3.3. **The crystal was optically excited by two collimated beams as in the shown two-side pumping scheme.**

This was due to a concern with crystal damage that could result from excessive optical power from the pump laser. These calculations were used to parameterize radius and absorption coefficients for purposes of optimizing experimental variables and possibly improving crystal growth parameters

such as doping concentration in the future. These calculation results will be presented in chapter 4.

3.2 The growth details of Ce^{3+}:$LiCaAlF_6$ by the μ-PD method

The Ce:LiCAF crystal is grown by the μ-PD method modified for fluoride crystal growth [3-6] as shown in Figure. 3.4, High purity (>99.99%) CeF, AlF_3, CaF_2, and LiF (Stella Chamita) were used as starting materials. They were thoroughly mixed and placed inside a graphite crucible. The crucible was charged up to 100 vol% powder of starting materials or about 5-20 vol% regarding the melt. The chamber was then baked at 600 °C for 1 hour in order to remove oxygen traces from the moisture of raw materials and adsorbates on the chamber surface. Simultaneously, the chamber is further evacuated to 10^{-5} Torr. After baking, the recipient is filled with a mixture of Ar and CF_4 until ambient pressure. Ar and CF_4 were used because they are not reactive with the graphite crucible. The crucible is then heated to a melting temperature of about 1450 °C. The crystal is grown with complete solidification of the melt charged in the crucible and a pulling rate of 0.1 mm/min.

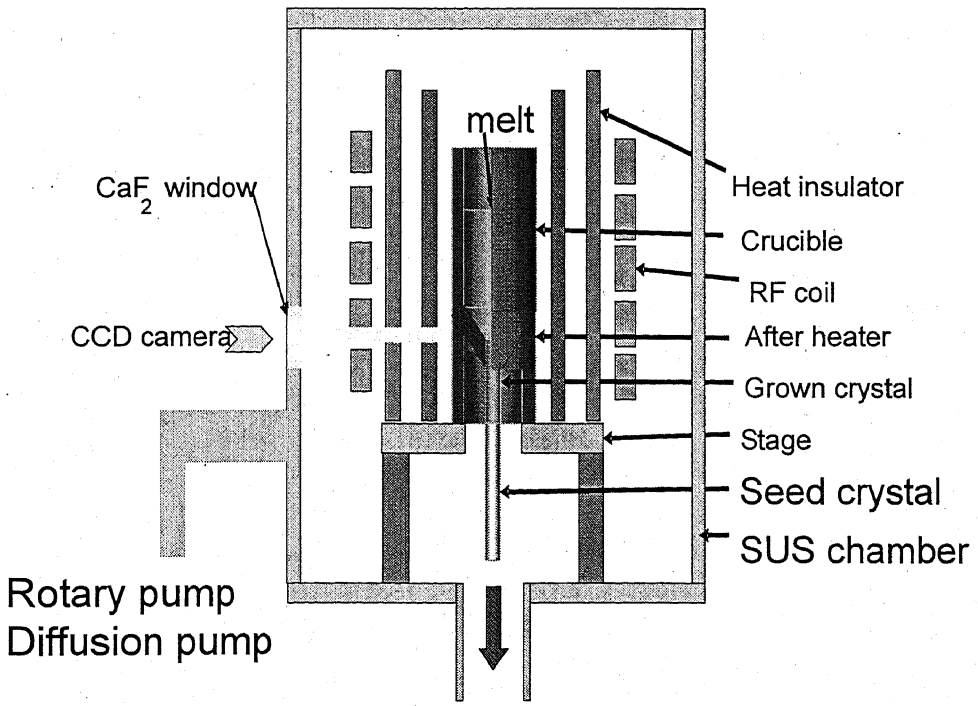

Fig. 3.4. **Schematic of Micro-pulling down growth system with RF heating.**

It was grown using a radio frequency (RF) heated μ-PD apparatus with a graphite crucible Temperature is raised by induction heating of a conductor coil by electromagnetic induction. Currents are induced in the coil and these currents cause heating. The frequency used is varied to control the amount of current and consequently, the temperature. The 30-mm long, 2-mm wide crystal used in the experiment is shown in Figure 3.5. Both ends of the as-grown crystal did not have any coating; the c-axis is in the growth direction. Note that the sides of the crystal are not polished.

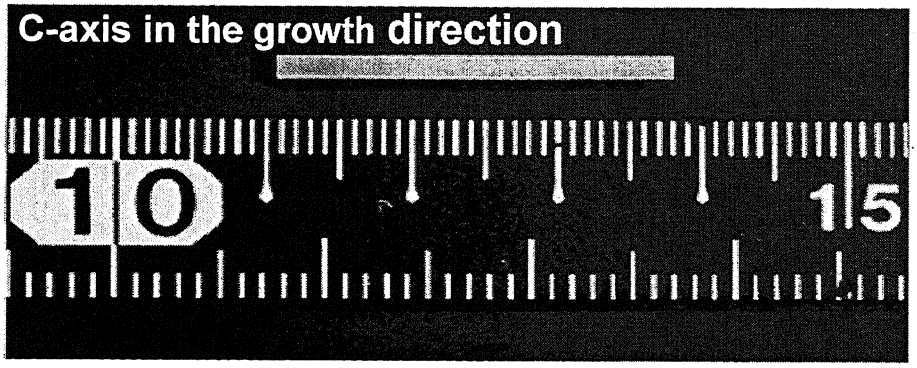

Fig. 3.5. **Photograph of as-grown Ce:LiCAF crystal. It is 30-mm long and 2-mm wide, and with sides unpolished.**

The UV optical properties of the Ce:LiCAF crystal were initially determined using a Jasco FP6500 spectrometer. Incident light hits the sample at the normal incidence. The transmitted light is then detected by a photomultiplier tube aligned collinearly with the source. The broad band excitation source was a 150 Watt Xenon lamp. The transmission spectrum is shown in Figure. 3.6, where the transmission dropped sharply at about 266 nm. Consequently, the absorption spectrum was calculated and it is shown in Figure. 3.7. The strong absorption at 266 nm suggests that this crystal is suitable for pumping with the fourth harmonic of a Nd:YAG laser.

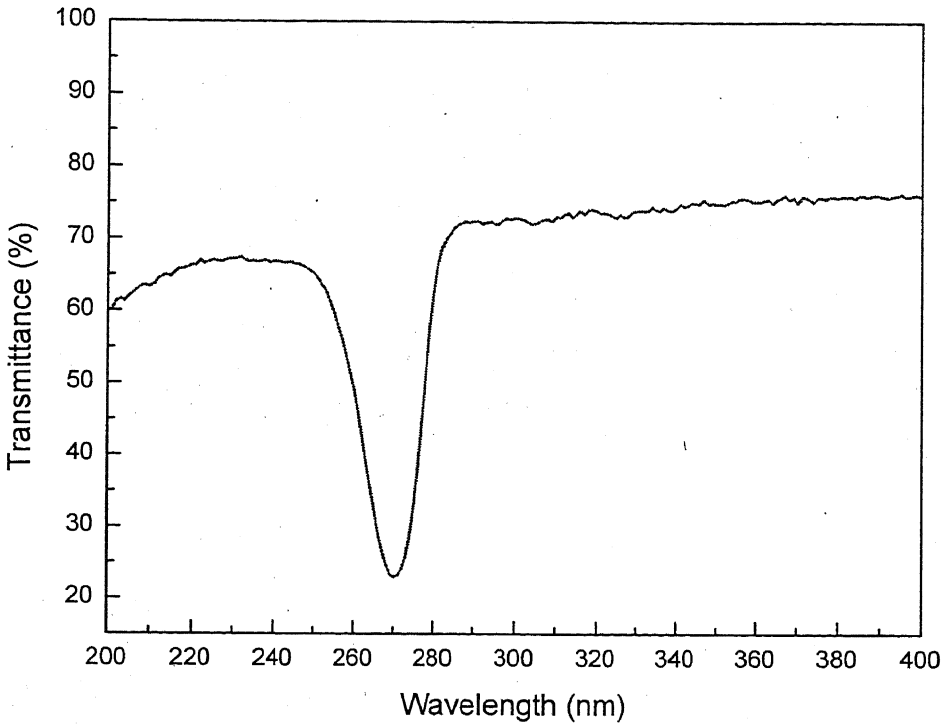

Fig. 3.6. **The transmittance spectrum of Ce:LiCAF.**

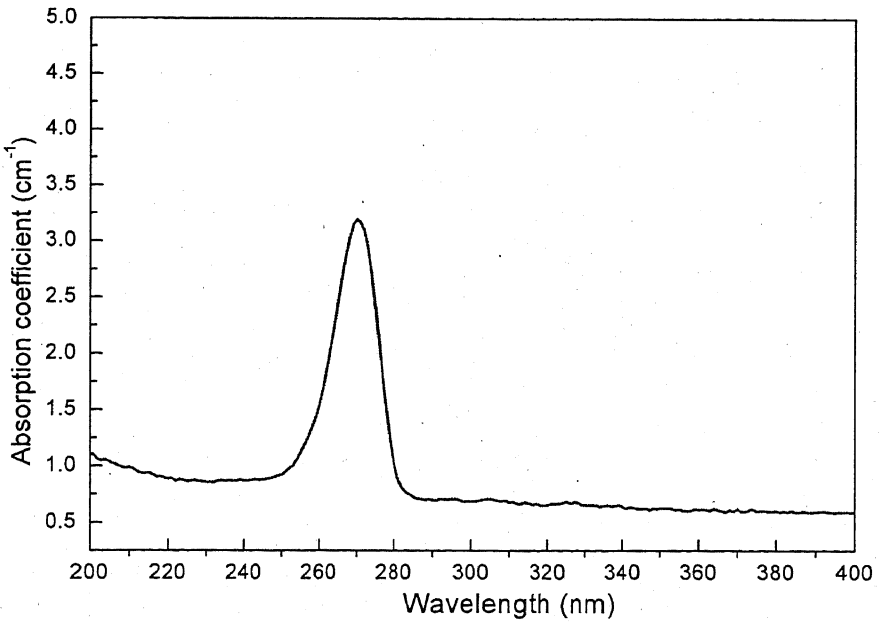

Fig. 3.7. **The absorption spectrum of Ce:LiCAF.**

3.3 The experiment setup of the Ce:LiCAF laser oscillator

The quality of the Ce:LiCAF crystal as a laser material was then evaluated. The slope efficiency determined by the dependence of the laser emission power on the average optical pump power is a standard measure of the quality of a laser material. The Ce:LiCAF crystal has a strong absorption band at 266 nm, and is therefore readily pumped by the 4th harmonics of Nd:YAG laser. For this study, a laser cavity was constructed as described below.

In the experiment, the crystal is simultaneously pumped on both sides by the fourth harmonics of two synchronized Nd:YAG lasers operating at 266 nm and 10 Hz repetition rate. Incident 266nm pulses have 5 ns pulse width. The schematic diagram and a photograph of the two-side pumping configuration of the laser cavity are shown in Figure. 3.8.

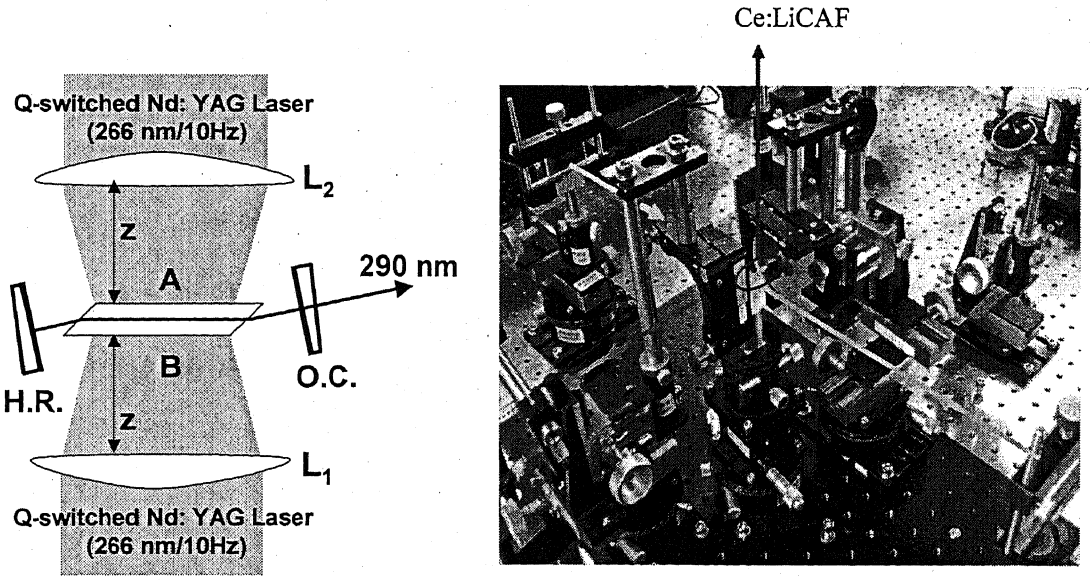

Fig. 3.8. **Schematic diagram of the Ce:LiCAF laser oscillator.**

This side – pumping scheme was due to a concern with crystal damage that could result from excessive optical power from the pump laser. The laser resonator is established by using a flat high reflector (H.R) with > 99% reflection at 290 nm and a flat output coupler (O.C.) with a 60% transmission at 290 nm. The length of the laser cavity is 6 cm. Cylindrical lenses, L_1 and L_2, both with focal lengths of 300 mm are used to individually focus the pump beams onto opposite sides of the crystal so that the cylinder axis is parallel to the side window of the crystal The Ce:LiCAF crystal grown by the method described previously (2 mm in diameter, and 30 mm long) was doped with 1mol% Ce^{3+} ions. The distance of the lens to the sample is set at 260 mm to ensure that the beam excites the entire side with sufficient fluence without ablating the crystal. The output energy is measured using a Gentec ED100 Joule meter. The dependence of the Ce:LiCAF laser energy with the increase in pump energy from 1mJ to 7 mJ was recorded.

The measured slope efficiency are presented and discussed in the next chapter

3.4 The experiment setup of the Ce:LiCAF laser oscillator using a Prismatic cell configuration

One way of possibly increasing the laser output power for the Ce:LiCAF laser oscillator is to design a multiple side pumping scheme. This will permit a more homogenous spatial distribution of the absorbed optical energy. Multiple pumping offers improved beam quality, ease of alignment, and reduced risk of damage to the crystal since the crystal can be pumped at a lower fluence for each side without compromising laser output energy.

This multiple side pumping design is achieved using two Ce mirrors (CeHR) that are highly reflecting at 266 nm. The mirrors are positioned at right angle with respect to each other. The optical pump is incident at a 45^0 angle with respect to the mirrors' normal. A schematic diagram of the optical geometry is shown in Figure. 3.9, where a cross-sectional view of the design is shown. As shown in the diagram, if the height of the incident pump is four times that of the crystal diameter, the Ce:LiCAF crystal can be placed at two independent positions such that it can be pumped a total of four times. This multiple pumping scheme utilizing the multiple reflections in the mirror geometry is similar in principle to a prismatic cell design that was previously employed in optically pumped dye lasers [7, 8].

As in the previous case, the laser resonator is established using the same set of mirror and coupler. The only difference is that in this case the distance of the cylindrical lens to the sample is set at 180 mm from the sample to specify the beam height to be four times that of the Ce:LiCAF crystal diameter. The segments of the pump beam labeled 1,2,3, and 4 in the diagram

will pump the top, right, left, and bottom of the crystal, respectively.

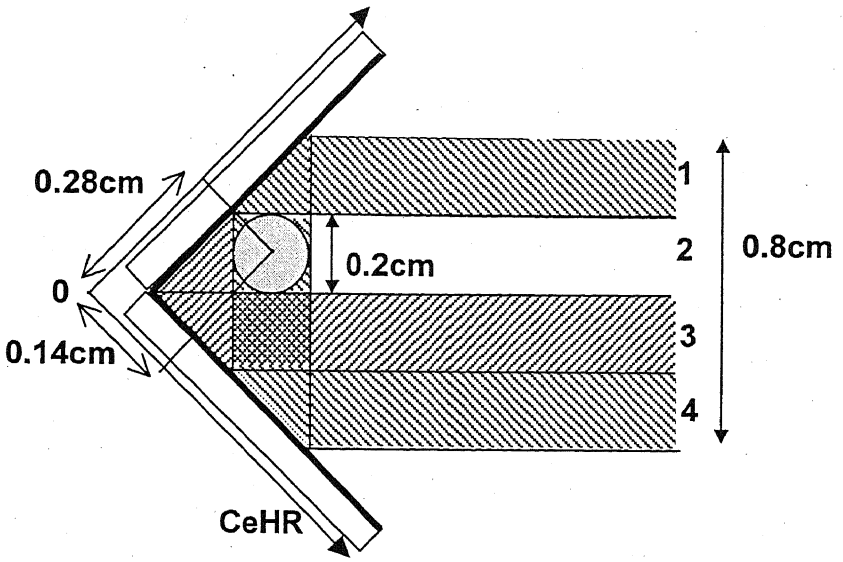

Fig. 3.9. **Schematic diagram of the Prismatic cell (side view).**

The measured slope efficiency are presented and discussed in the chapter 4.

3.5 Reference

1. Max Born and Emil Wolf. Principles of Optics. Cambridge. (1980), 38.
2. William T. Silfwast. Laser fundamentals, second edition, 234.
3. A. Novoselov, A. Yoshikawa and T. Fukuda. Current Topics in Cryst. Growth Res. **7**, (2004), 87
4. A. Yoshikawa, M. Nikl,G. Boulon, and T. Fukuda, Opt. Mater. **30**, (2007), 6.
5. A. Yoshikawa, T. Satonaga, K. Kamada, H. Sato, M. Nikl, N. Solovieva, and T. Fukuda. J. Cryst. Growth. **270**, (2004), 427.
6. A. Yoshikawa, K. Kamada, M. Nikl, K. Aoki, H. Sato, J.Pejchal, and T. Fukuda. J. Cryst. Growth. **285,** (2005), 445.
7. D. S. Bethune., Appl. Optics. **20**, (1981), 1897.
8. P. Smon and N. Juhasz. J. Phys. E; Sci. Instrum. **18**, (1985), 829.

Chapter 4

Results and discussion

4.1 Calculation results

4.1.1 Absorption profile

The contour plot of the cross-sectional absorption profile is presented in the 3-dimensional plot shown in Figure. 4.1.1. For ease of visualization, the contour plot is compared with the crystal cross-sectional diagram that was shown earlier in Fig. 3.2. Note that the vertical-axis is the absorbed energy axis, illustrating that the highest absorption is at regions near the crystal's illuminated surface. The absorbed energy profile then decreases according to Beer-Lambert's equation, except for some regions inside the crystal where the electric field lines intersect due to refraction and where we expect a slight increase in the absorption.

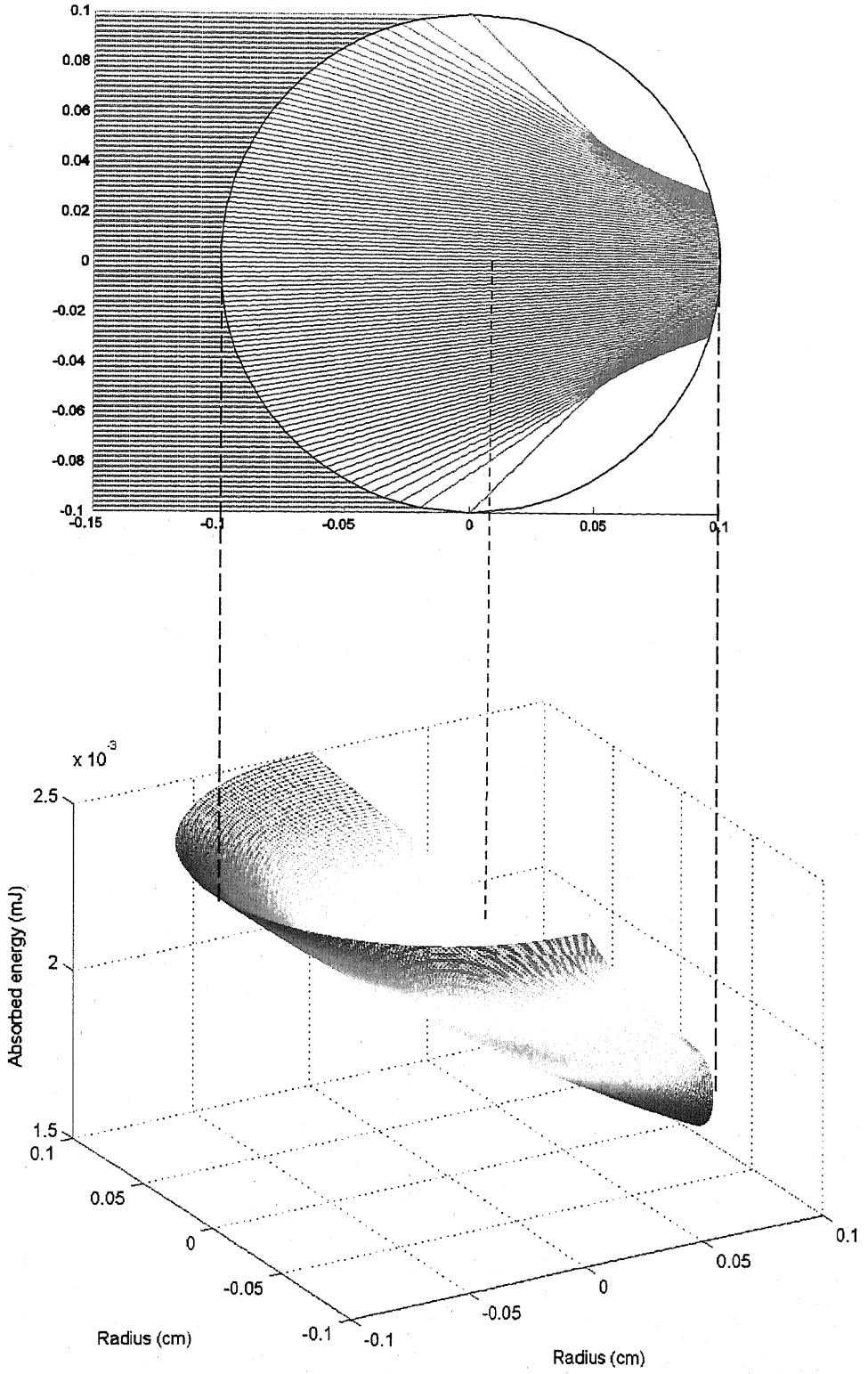

Fig. 4.1.1. **The absorption profile for one-side pumping in three-dimension plot**

To estimate the dependence of the absorbed energy on the radial position inside the crystal, I solved equation (3.4).

The definition of radial position is illustrated in Figure. 4.1.2. The absorbed energy at concentric semicircular regions for different radial distances from the center was calculated. Moreover, these semicircular regions were divided into two domains; namely, those belonging to the "0 to -R" region and those in the "0 to +R" region. This allows for the mapping of the radial profile of the absorbed energy in the crystal from –R to +R.

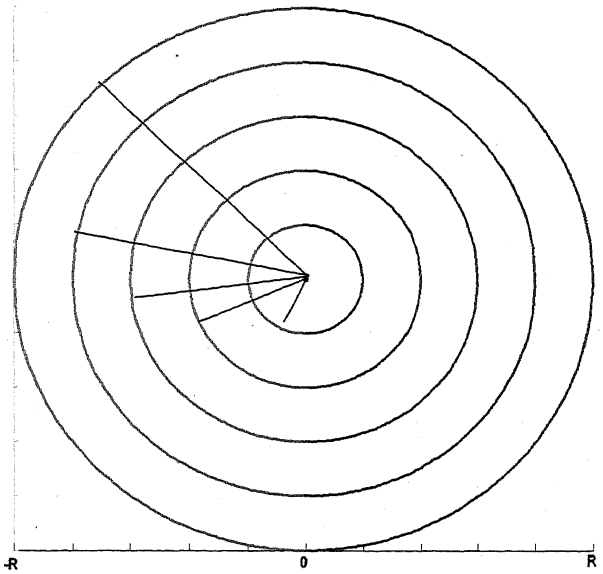

Fig. 4.1.2. **Illustration of the radial position in the crystal as defined in the text**

With one side pumping, the pump energy is 100 mJ while with two sides pumping; the pump energy is 50 mJ for each side. The radius and absorption coefficient of the crystal were specified to be 0.1 cm and 2.5cm^{-1}, respectively. These are the actual experimental values for the crystal radius and absorption coefficient (at 266 nm). The results of the calculation are shown in Figure. 4.1.3.

The absorbed energy at +0.1 radial position was found to be 62% of the absorbed energy at -0.1 radial position. This translates to about 38% incident radiation being absorbed by the crystal. In addition, although the radial profiles for both the one-side and two-side pumping schemes are similar, the two-side pumping case is more symmetric. As will be discussed in more detail later on, this symmetric profile is advantageous in terms of crystal damage concerns, electric field distribution uniformity, and possibly laser output beam profile.

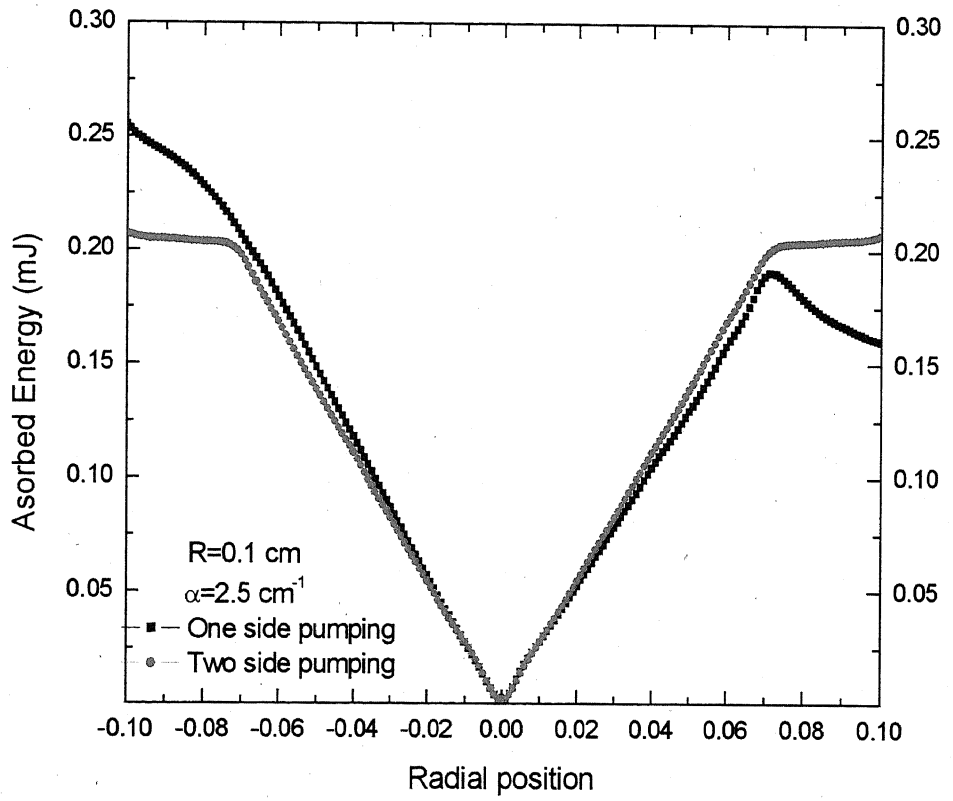

Fig. 4.1.3. **The absorption profile dependence on the radial position of the crystal.**

4.1.2 The dependence of absorbed energy on radius

I defined the ratio of the absorbed energy at the crystal center (E_0) and the absorbed energy at the surface (E_e) to be E_0/E_e. This gives a measure of the absorbed energy between the center of the crystal and at the edge region. It also provides information on the spatial non-uniformity of the absorbed energy in the crystal. The radius of the crystal was varied from 0.1 to 1 cm. The absorption coefficient is 2.5 cm^{-1} and the pump energy is 100 mJ for one side pumping. The result is shown in Figure. 4.1.4. The E_0/E_e decreased when radius is increased. However, the E_0/E_e is almost unchanged with radii values larger than 0.5 cm. This suggests that for crystal radii greater than 0.5 cm , the radius is no longer a factor in the non-uniformity of the absorbed energy.

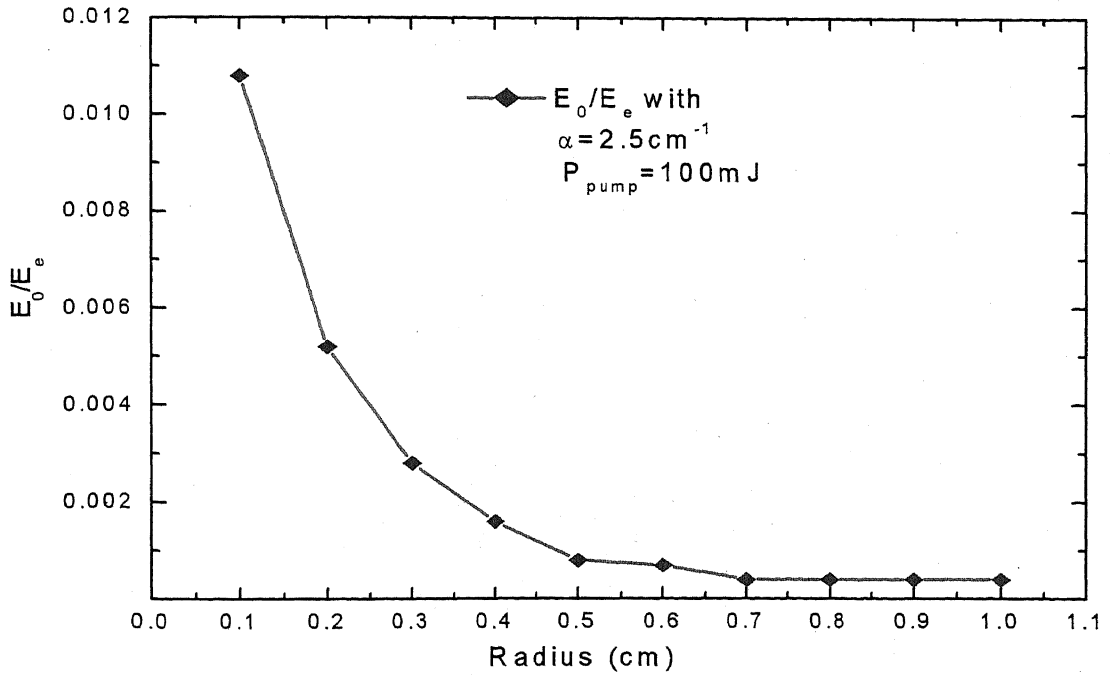

Fig. 4.1.4. **The dependence of the ratio of the absorbed energy between the center and the surface of the crystal on the radius.**

4.1.3 The dependence of absorption profile on absorption coefficient

The dependence of the radial position profile of the absorbed energy (E_0/E_e) inside the crystal for different absorption coefficients was also investigated. In addition, the radial profile for one-side and two-side pumping are compared. Figure. 4.1.5(a) shows the radial position profile for one-side pumping for different absorption coefficients namely, 0.5, 1, 2, 2.5, and 3 cm^{-1}. It must be noted that since this is for one-side pumping, the profile must not be symmetric about R=0 see Figure 4.1.3. Since the variation of E_0/E_e is considered, the radial profile was plotted in log scale for clarity. This diminished the perceived asymmetry of the radial profiles but clearly showed the differences of the E_0 value.

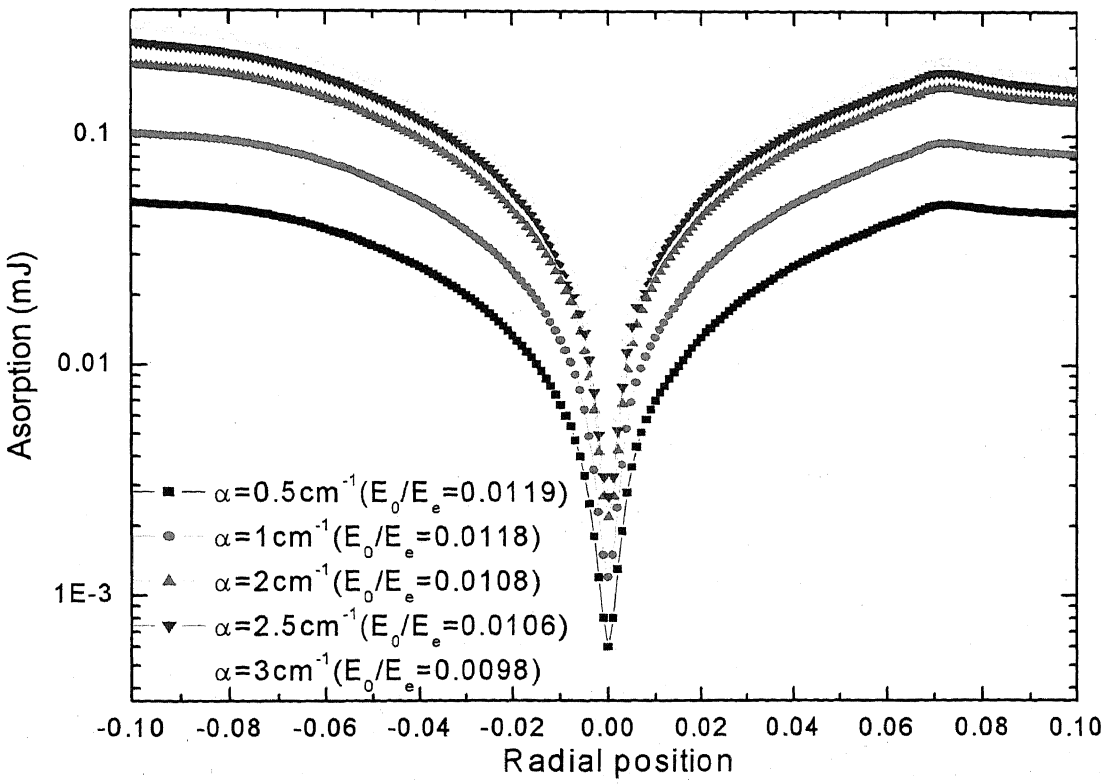

Fig. 4.1.5(a). **Absorption profile for one side pumping**

According to the calculation results, the E_0/E_e becomes more pronounced for higher absorption coefficients. Thus, for one-side pumping and with the 2.5 cm^{-1} absorption coefficient for the actual sample, the E_0/E_e value suggests that the absorbed energy at the crystal center is very low compared with the edge region.

For the two-side pumping, on the other hand, the symmetry of the radial profiles of the absorbed energy is easily seen as shown in Figure. 4.1.5(b). Moreover, the general values of E_0/E_e are much higher in this case. This means that the absorbed energy at the center is higher than in the one side-pumping scheme. Thus, a more uniform spatial distribution of absorbed energy in the crystal cross section should be expected. In addition, the variation of E_0/E_e with the absorption coefficient is not as drastic as in the one-side pumping case. This suggests that two-side pumping is more versatile in efficiently exciting crystals with different absorption coefficients. Finally, in the interest of laser output, beam profile quality of the two-side pumping method should yield a more symmetric beam profile output.

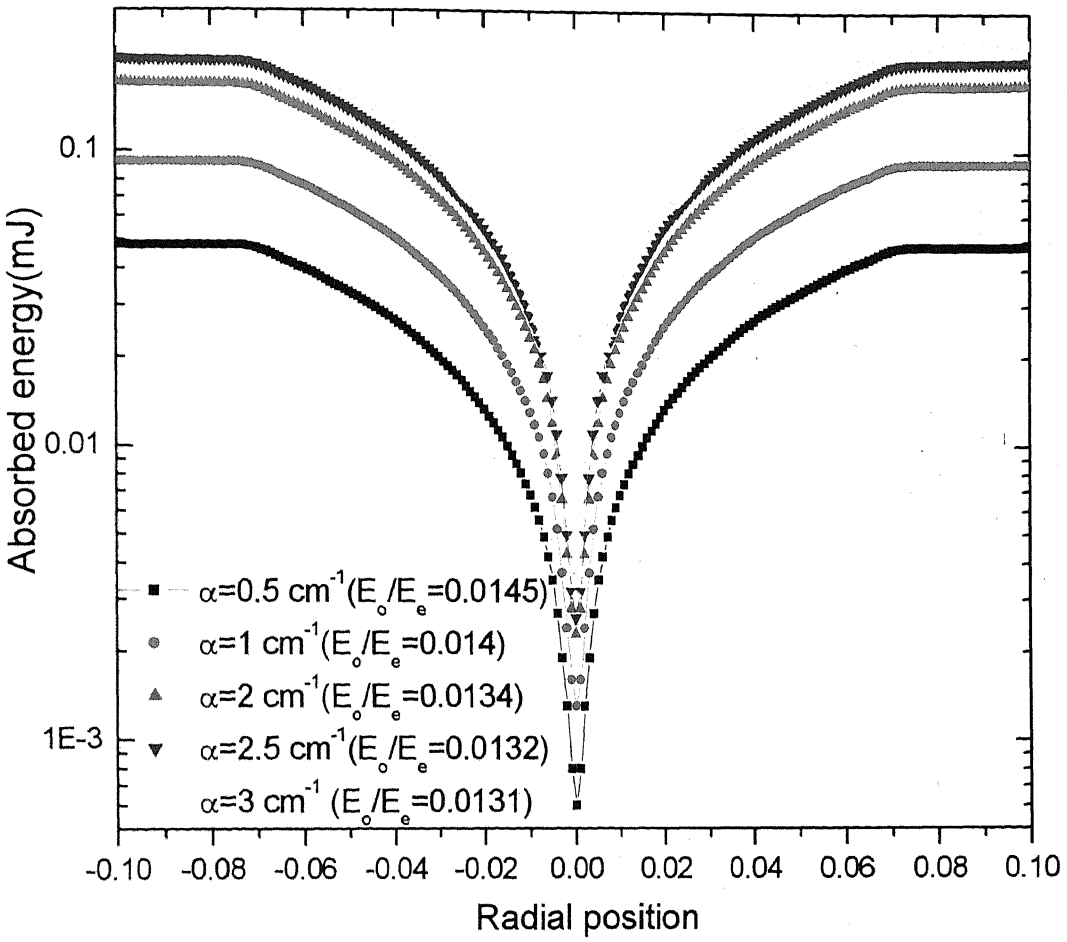

Fig. 4.1.5(b). **Absorption profile for two-side pumping**

4.1.4 The dependence of absorption ratio on radius

I also estimated the dependence of the absorption ratio η on the radius of the crystal for different absorption coefficients. The results of the calculation are shown in Figure. 4.1.6, where the parameterization of the absorption coefficient is demonstrated for radii values ranging from 0.1 cm to 1 cm. The dependence of the absorption ratio with radius appears to be linear for small values of the absorption coefficient. As the absorption coefficient is increased, however, the dependence becomes exponential, making it more agreeable with what is expected from Beer-Lambert's equation. For absorption coefficients equate to 2.5 cm^{-1} and above, the absorption ratio begins to saturate at a radius of about 0.5 cm. Note that according to previous measurements, the actual absorption coefficient of the sample at 266 nm is 2.5 cm^{-1}. It can be inferred that for the experimental conditions used in this work, the optimum crystal radius should be 0.5 cm. A larger crystal radius is not required to have an improvement in the absorption ratio.

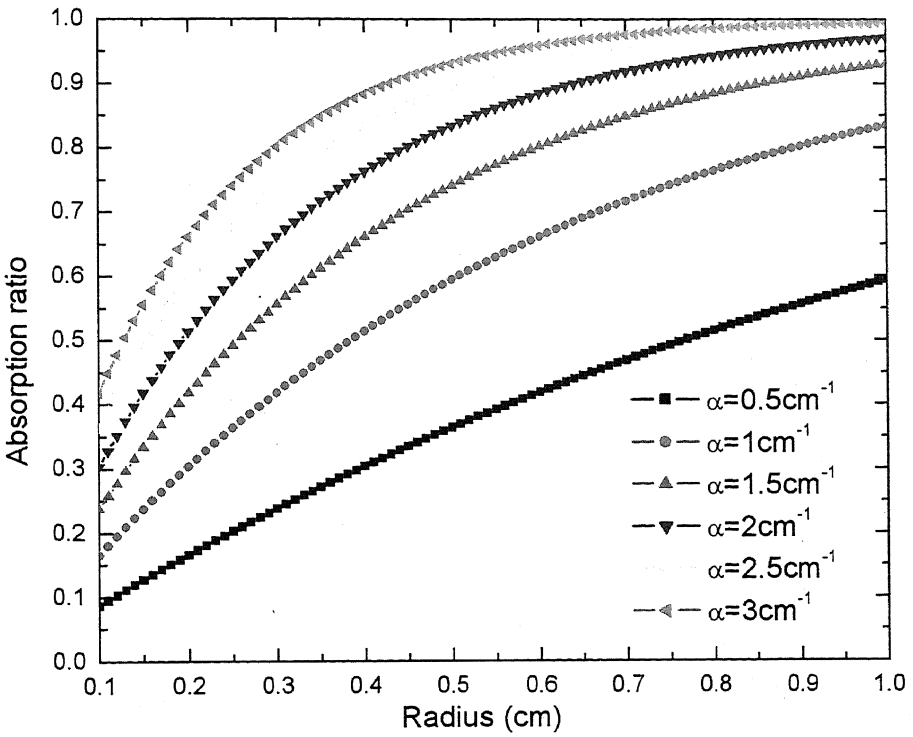

Fig. 4.1.6. **The dependence of absorption ratio on the radius of crystal for different absorption coefficients.**

4.1.5 The dependence of absorption ratio on absorption coefficient

Figure. 4.1.7 parameterizes the radius as a function of absorption coefficient. The results agree with Fig. 4.1.6. The absorption ratio is again shown to behave exponentially for large crystals and a saturation condition is observed for high absorption coefficient values. Again, for the sample that was studied, the optimum radius is found to be about 0.5 cm. In this experiment, however, the radius of the crystal was only 1 mm. Thus, at present, the crystal sample properties are far from optimal.

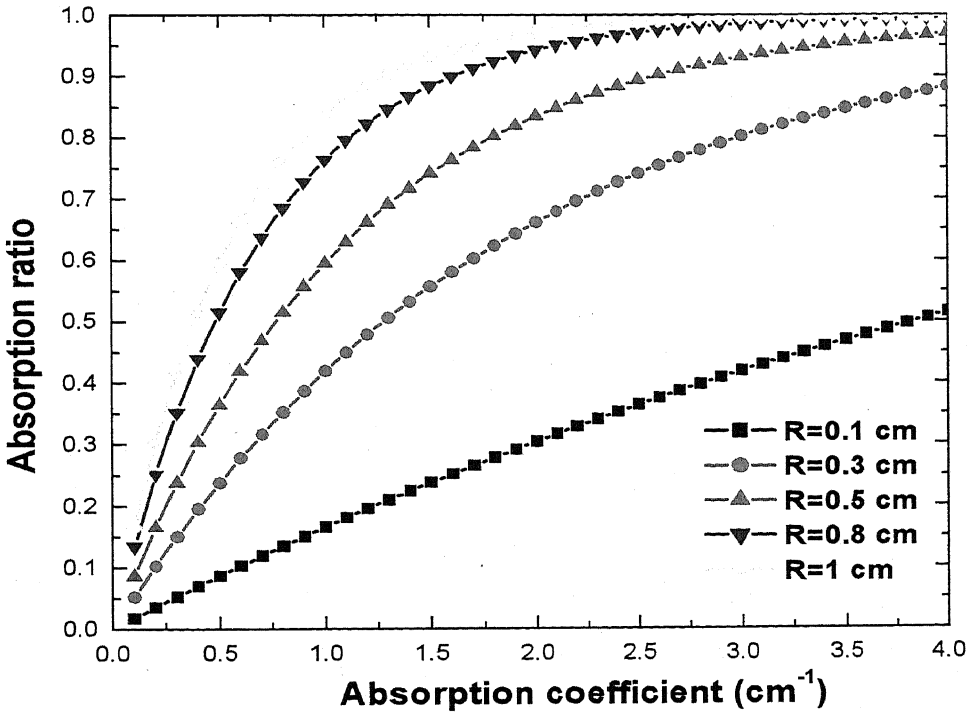

Fig. 4.1.7. **The dependence of absorption ratio on the absorption coefficient for different radius of crystal.**

4.2 Experimental results

4.2.1 Lasing from an as-grown Ce:LiCAF

Figure. 4.2.1 shows the measured laser oscillator output energy as a function of the absorbed pump energy for the one- and two-side pumping configurations shown in the experiment setup in Chapter 3. The output energy remained linear with absorbed energy.

With the as–grown Ce:LiCAF crystal I achieved a slope efficiency of 10% for one and two–side pumping. Slope efficiency is an important property of a laser. It is obtained by plotting the laser output power against the input pump power. Above the lasing threshold, the resulting curve is usually close to a straight line. The slope efficiency is the slope of this line. The slope efficiency and output energy for each side in the one-side pumping scheme are comparable, indicating that the emission condition for individual sides is similar. For two-side pumping, the slope efficiency and oscillator output energy are almost the same with that of the one-side pumping configuration. Equally distributing the total pump energy to two sides yields the same output energy as pumping one side with an equivalent energy. For example, pumping one side with 3mJ would yield the same output as pumping both sides with 1.5 mJ each. Considering that the crystal is homogeneously doped, the total energy absorbed by both sides of the crystal in the two-side pumping configuration is almost the same as the energy absorbed by one side when all of this total energy is directed onto just one side. Therefore, the total output energy and hence the slope efficiency would almost be the same.

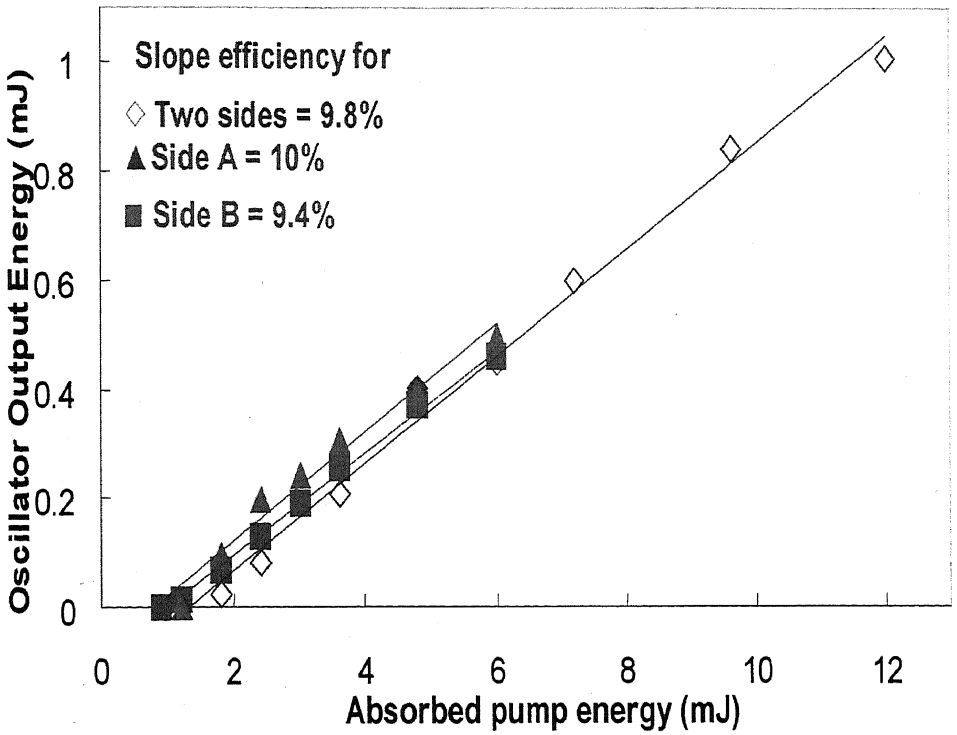

Fig. 4.2.1. **Oscillator output energy for as-grown crystal with 10% slope efficiency of Ce:LiCAF laser.**

This implies that two-side pumping is more advantageous than one-side - pumping by reducing damage to the crystal. Moreover, the lasing threshold can be estimated from the slope efficiency plot. The lasing threshold is the lowest excitation level at which a laser's output is dominated by stimulated emission rather than by spontaneous emission. Below the threshold, the laser's output power rises slowly with increasing excitation. Above threshold, the slope of power vs. excitation is orders of magnitude greater. Above the threshold, the laser is said to be lasing. The energy and fluence threshold were consequently determined to be 1.5 mJ and 6 mJ/cm^2, respectively. Fluence threshold is pump energy per unit area at the lasing threshold. From the plot, the laser threshold for one side pumping is about 1 mJ and a fluence of about 4 mJ/cm2 while the laser threshold for two-side

pumping is higher than one side pumping. For two-side pumping the total pump energy of 1 mJ would imply 0.5 mJ pumping on each side of the crystal, consequently decreasing the fluence. Since the pump fluence is below threshold fluence, the absorbed energy is not sufficient for lasing to occur.

4.2.2 Lasing from an as-grown Ce:LiCAF using Prismatic-cell configuration

For improved laser performance of the as-grown Ce:LiCAF crystal, the prismatic cell configuration, described in Chapter 3, was used. As shown in Fig. 4.2.2, a slightly lower slope efficiency of 8.9% was measured for this configuration. Although a higher slope efficiency was expected, this was not observed experimentally. This might be attributed to losses from the two Ce mirrors that were used. Moreover, alignment errors might have further contributed to the slightly lower slope efficiency that was observed.

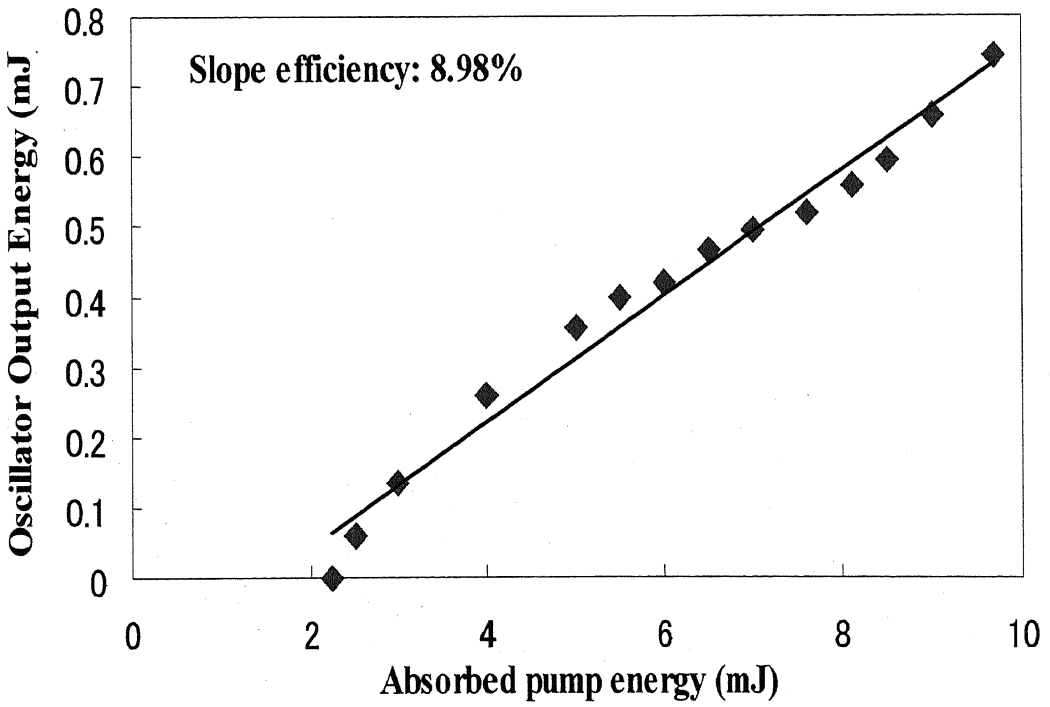

Fig. 4.2.2. **Ce:LiCAF laser oscillator output energy for as-grown crystal using Prismatic-cell with a 8.9% slope efficiency.**

4.2.3 Lasing from Brewster cut Ce:LiCAF

For improved laser performance of the Ce:LiCAF crystal, both ends of the sample crystal were cut at a Brewster angle about 60 degree. In general, when the light moves between two media of differing refractive index, some of it is reflected at the boundary. At one particular angle of incidence, however, light with a particular polarization cannot be reflected. This angle of incidence is called the Brewster's angle. The polarization that cannot be reflected at this angle is the polarization for which the electric field of the light waves lies in the same plane as the incident ray and the surface normal (i.e. the plane of incidence). Light with this polarization is said to be p-polarized, because it is parallel to the plane. The resulting fluorescence when the crystal is pumped by 266 nm is randomly polarized. Fluorescence exiting the Brewster cut ends will be dominantly p-polarized. The Brewster cut end therefore facilitates optimum feedback of the p-polarized output to the crystal. Correspondingly, the laser output would be p-polarized. The crystal is shown in Figure. 4.2.3.

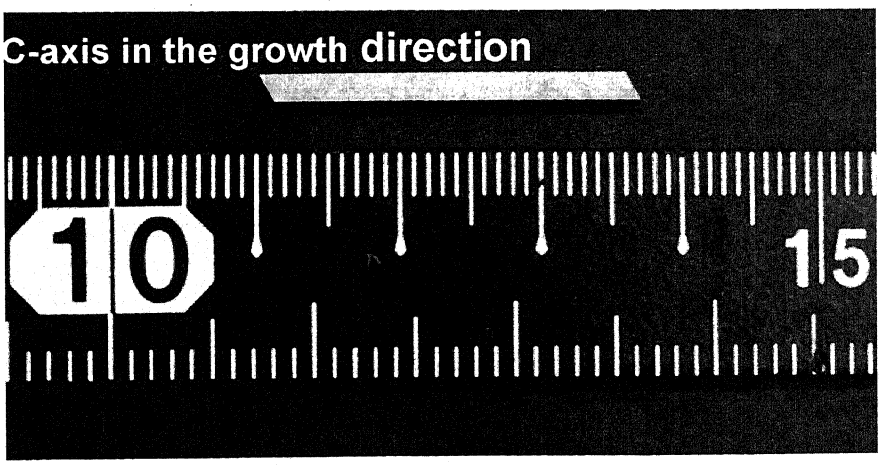

Fig. 4.2.3. **Brewster cut Ce:LiCAF crystal with 30-mm long and 2-mm wide, and unpolished**

Employing the same procedure, I was able to achieve a slope efficiency of 23% for one-side and two-side pumping configurations as shown in Figure. 4.2.4. A maximum output pulse energy of 1 mJ at 290 nm is achieved with an absorbed pump energy of 6 mJ. The lasing threshold is 2.5 mJ, which corresponds to a threshold fluence of 10 mJ/cm^2.

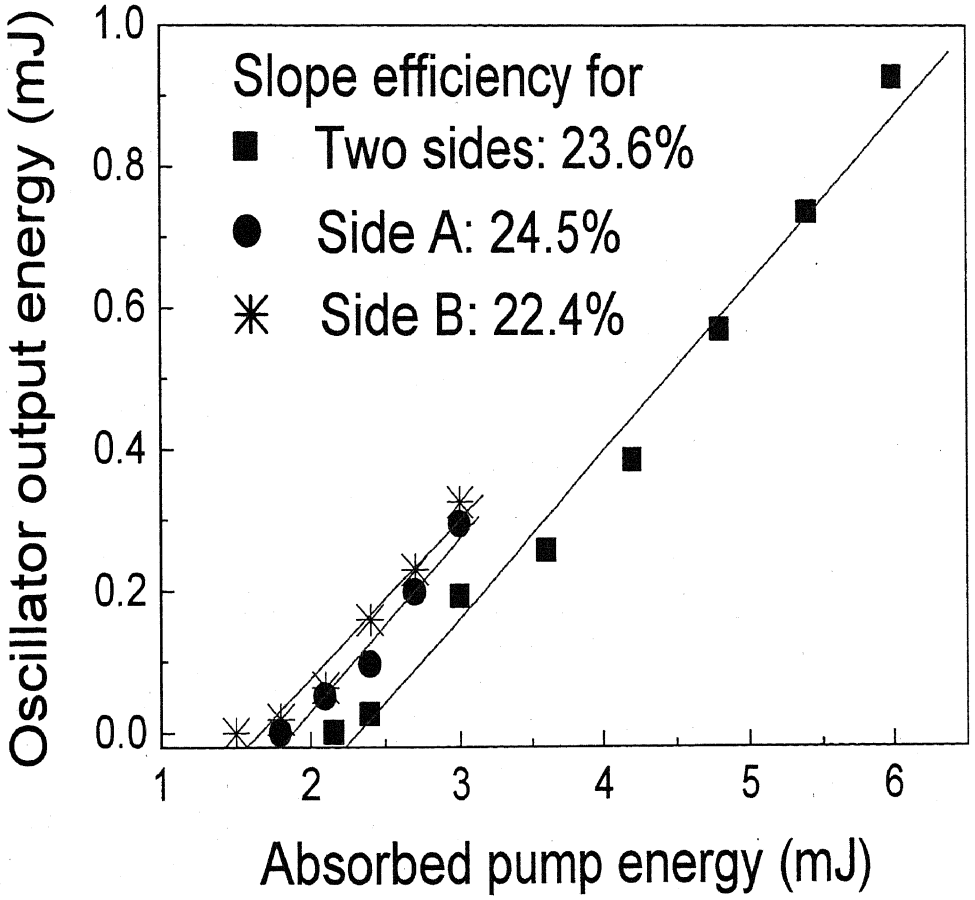

Fig. 4.2.4. **Oscillator output energy with 23% slope efficiency. Independent transmission measurements with the polished crystal reveal that roughly 10% of the pump energy is absorbed.**

I expected the lasing threshold and fluence threshold to be smaller for the Brewster-cut sample. However, this was not observed in our experiment. This may be attributed to the measuring instrument's resolution,

lower-limit sensitivity and other factors. The main purpose of this procedure, however, is the verification that a Brewster cut laser material would, indeed, yield an improved slope efficiency. Previously, CZ grown, 15-mm diameter Ce:LiCAF is reported to have a slope efficiency of 39% [2-5]. From this, it can be said that the quality of μ-PD grown Ce:LiCAF is rather comparable to the CZ grown crystal.

Finally, the typical spectrally and temporally resolved streak-camera image of the Ce:LiCAF laser output pulse is given in Figure. 4.2.5. The emission at 290 nm has a pulse width of approximately 4 ns and a band width (full width at half maximum) of 2 nm.

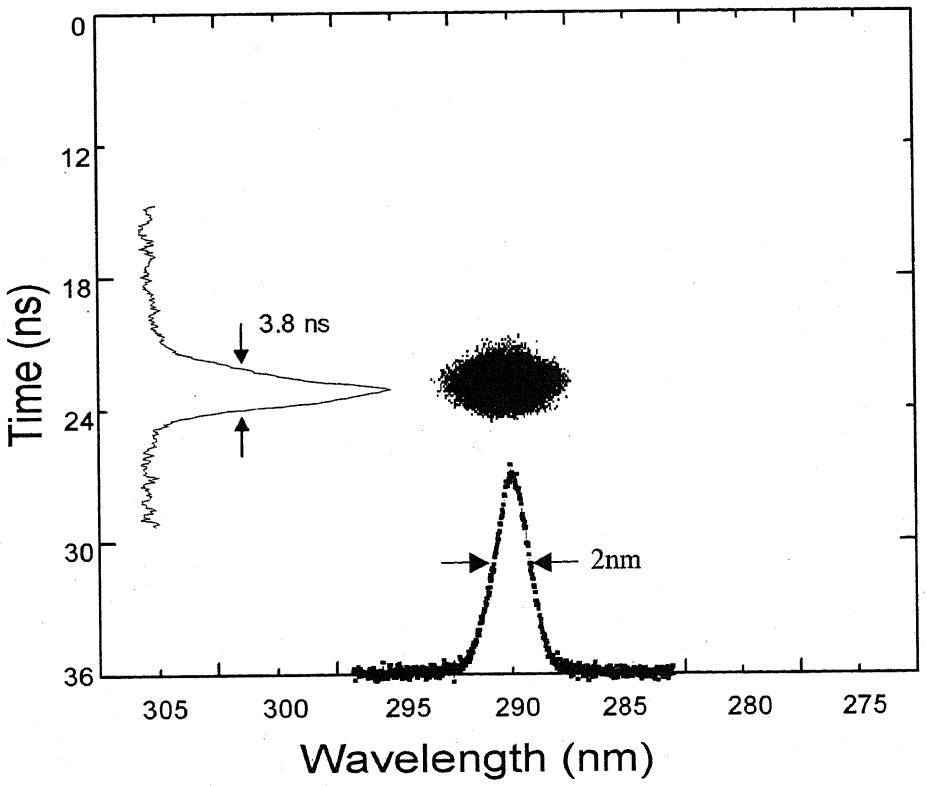

Fig. 4.2.5. **Temporally and spectrally resolved streak-camera image of Ce:LiCAF laser.**

4.3 References

1. Minh H. Pham, M. Cadatal, T. Tatsumi, A. Saiki, Y. Furukawa, T. Nakazato, E.Estacio,N. Sarukura, T. Suyama, K. Fukuda, K. Jin Kim, A. Yoshikawa, and F. Saito, Jpn. J. Appl. Phys. **47**, (2008), 5605.
2. Z.Liu, S. Izumida, H. Ohtake, N. Sarukura, K. Shimamura, N. Mujilatu, S. L. Baldochi and Fukuda. Jpn. J. Appl. Phys, **37,** (1998), L1318.
3. K. Shimamura, S. L. Baldochi, N. Mujilatu, K. Nakano, Z. Liu, N. Sarukura, and T. Fukuda, J. Cryst. Growth. **211,** (2000), 302.
4. K. Shimamura, N. Mujilatu, K. Nakano, S. L. Baldochi, Z. Liu, H. Ohtake, N. Sarukura, and T. Fukuda, J. Cryst. Growth. **197**, (1999) 896.
5. K. Shimamura, H. Sato, A. Bensalah, V. Sudesh, H. Machida, N. Sarukura, and T. Fukuda, J. Cryst. Growth. **36**, (2001) 801.

Chapter 5

Conclusions and Prospects

The μ-PD down method has been increasingly used for the growth of solid-state optical materials. Prior to this work, there has only been one report of laser emission from a crystal grown by this method. A 1064 nm laser emission with maximum output power of 10W and a 22% slope efficiency was reported from a Nd:YAG single crystal grown by the μ-PD method. Because of the modest slope efficiency and the lack of follow-up work, the μ-PD method was considered not suitable for growing high quality laser-grade crystals. With the improvement of the crystal growth method parameters such as optimal crystal diameter and the best doping concentration for optimizing the absorption coefficient, a laser quality Ce:LiCAF has been grown and we were able to demonstrate the first ultraviolet laser from μ-PD method grown fluoride crystal. The flexibility and lower cost of this crystal growth scheme will drastically reduce the cost of crystal growth.

In conclusion, successful lasing operation at 290 nm was demonstrated for μ-PD grown Ce: LiCAF cylindrical crystal using the fourth harmonics (266nm) of an Nd:YAG laser as optical pump. This is a very good demonstration of the capability of the μ-PD method in growing laser-grade crystals, contrary to initial speculatoins. Initially, numerical methods were used to evaluate the optimum radius and absorption coefficient of the sample and to map the radial profiles of the absorbed energy and absorption ratio inside the crystal. For 266 nm optical pumping and given the absorption

coefficient of the material at this wavelength, the optimum crystal radius was determined to be 0.5 cm. This information may be useful for future growth parameter considerations such as crystal size and doping concentration.

This multiple side-pumping scheme utilizing the multiple reflections in the mirror geometry described in Section 3.4, can offer an improved laser output beam quality due to more uniform electric field distribution in the crystal. It could also reduce the risk of damage in the crystal. Moreover multi-pass pumping will yield high power. This pumping geometry is similar in principle to a prismatic cell that was previously used in dye laser and was applied for the first time in this work to a solid-state laser system. This will be especially important in design high energy optically pump Ce:LiCAF laser.

More importantly, a laser oscillator was designed for a 0.1 cm cylindrical crystal and the slope efficiencies were compared for one- and two-side pumping configurations. The slope efficiencies for as-grown and Brewster-cut samples were also studied. Results showed that the slope efficiency did not change for one or two-side pumping. The latter, however, is preferred since it greatly reduces the risk of optical damage to the Ce:LiCAF crystal. The experiment also showed that the slope efficiency improved from 10% to 23% when the sample's output windows were cut as being a Brewster angle. It should be noted that the samples that were studied in this work did not have polished sides, thus, explaining the relatively low slope efficiency values. Moreover, the sample radius was only 0.1 cm; much smaller than the numerically determined optimum radius was determined to be 0.5 cm, in the Figure. 4.1.6. In the future, these modifications could be incorporated to yield

more impressive results. The point of this work, however, is the proof-of-concept demonstration that μ-PD growth is feasible as a growth method for fluoride-based UV laser materials. The advantages offered by μ-PD method could drastically reduce growth costs and will also open up possibilities of simple and compact UV laser sources.

In the aspect of laser design, a four-side pumping scheme using a prismatic cell design could be employed to further improve the uniformity of the absorbed energy and to further reduce optical damage. Finally, owing to its absorption band at 266 nm, it may be used as a gain medium for amplifying the third harmonics (290 nm) of a Ti:Sapphire laser while pumping the crystal with the fourth harmonics of an Nd:YAG laser at 266 nm. With the available Ce:LiCAF crystal, approximately twenty times gain is expected for a 100 μJ, 2.6 ps seed pulse.

ACKNOWLEDGEMENT

I would like to express my sincere gratitude and appreciation to my adviser. Prof. Nobuhiko Sarukura for scientific guidance throughout the study and for providing a chance of studying in the Graduate University for Advanced Studies and Institute for Molecular Science.

I am also indebted to Prof. Akira Yoshikawa and Dr. Kentaro Fukuda for useful discussions and providing the Ce:LiCAF crystal used in my experiments.

I would like to thank to Dr. Elmer Estacio, Ms. Marilou Macasieb Cadatal, and Dr. Yusuke Furukawa for assisting me with my experiment and helpful discussions for improving my work.

I wish to thank to Ms. Satomi Suzuki and Ms. Junko Seto for taking care of necessary documents as well as for their encouragements.

My life in Japan wouldn't have been as enjoyable had not it been for my colleagues, for this I thank Dr. Tomoharu Nakazato, Dr. Shigeki Saito.

I express my gratitude to Prof. Nguyen Dai Hung, Vietnamese academy of science and technology, Institute of Physics for his kind advice.

Finally, I would like to thank to my family for their love and unmeasured support.

Publication List

Publication in Journal

1. **Minh H. Pham**, Marilou M. Cadatal, Toshihiro Tatsumi, Ayumi Saiki, Yusuke Furukawa,Tomoharu Nakazato, Elmer Estacio, Nobuhiko Sarukura, Toshih Toshihisa Suyama, Kentaro Fukuda, Kyoung Jin Kim, Akira Yoshikawa, and Fumio Saito. "Laser Quality Ce^{3+}:$LiCaAlF_6$ Grown by the Micro-Pulling Down Method", Jpn. J. Appl. Phys. **47**, (2008), 5605.
2. Elmer Estacio, Shigeki Saito, Tomoharu Nakazato,Yusuke Furukawa, Nobuhiko Sarukura, Marilou Cadatal, **Minh Hong Pham**, Carlito Ponseca. Jr, Hiroshi Mizuseki, and Yoshiyuki Kawazoe. "Birefringence of β-BaB_2O_4 crystal in the terahertz region for parametric device design". Appl. Phys. Lett. **92**, (2008), 090116.

International conference

3. M. Cadatal, **M. Pham**, Sono, E. Estacio, H. Murakami, Y. Fujimoto, Y. Seo , T. Tatsumi, N. Sarukura, M. Nakatsuka, K. Fukuda, A. Yoshikawa and T. Fukuda, "Comparison of vacuum ultraviolet (VUV) fluorescence from Nd^3+ doped LaF_3 and $YLiF_4$ " Oyo Butsuri Gakkai Gakujutsu Koen Yokoshu, **67**, 2006, 985
4. Marilou M. Cadatal, **Minh H. Pham**, Toshihiro Tatsumi, Ayumi Saiki , Yusuke Furukawa, Elmer Estacio, Nobuhiko Sarukura, Toshihisa Suyama, Kentaro Fukuda, Kyoung Jin Kim, Akira Yoshikawa, and Fumio Saito. "Ce^{3+}:$LiCaAlF_6$ Laser Quality Grown by the

Micro-Pulling Down Method and its Ultraviolet Lasing Properties", Advanced Solid-State Photonics (Optical Society of America), Nara, Japan January 27-30, 2008, WB18.

5. Marilou M. Cadatal, Young-Seok Seo, Toshihiro Tatsumi, **Minh Hong. Pham**, Carlito Ponseca Jr. Shingo Ono, Elmer Estacio, Yusuke Furukawa, Hidetoshi Murakami, Yasushi Fujimoto, Nobuhiko Sarukura, Masahiro Nakatsuka, Kentaro Fukuda, Rayko Simura, Toshihisa Suyama, Akira Yoshikawa, and Tsuguo Fukuda, "Nd^{3+}: $(La_{1-x},Bax)F_{3-x}$ grown via Micro-PD as New vacuum Ultraviolet scintillator and Potential Laser material". Conference on Lasers and Electro-Optics Pacific rim, Seoul, south Korea, August 27- September, **2**, 2007, Th E3-2.
6. Marilou M. Cadatal, Young-Seok Seo, Toshihiro Tatsumi, **Minh Hong. Pham**, Carlito Ponseca Jr. Shingo Ono, Elmer Estacio, Yusuke Furukawa, Hidetoshi Murakami, Yasushi Fujimoto, Nobuhiko Sarukura, Masahiro Nakatsuka, Kentaro Fukuda, Rayko Simura, Toshihisa Suyama, Akira Yoshikawa, and T. Fukuda, "Nd^{3+}: $(La_{1-x},Bax)F_{3-x}$ Grown by Micro-PD Method as New Vacuum Ultraviolet Scintillator and Potential Laser Material". Fifth International Conference in Inertial Fusion Sciences and Applications, Kobe, Japan, September 9-15, 2007, Fpo53.
7. Marilou M. Cadatal, Young-Seok Seo, Toshihiro Tatsumi, **Minh Hong. Pham**, Carlito Ponseca Jr. Shingo Ono, Elmer Estacio, Yusuke Furukawa, Hidetoshi Murakami, Yasushi Fujimoto, Nobuhiko Sarukura, Masahiro Nakatsuka, Kentaro Fukuda, Rayko Simura, Toshihisa

Suyama, Akira Yoshikawa, and T. Fukuda, "Investigation of Nd3+: (La1-x,Bax)F3-x as New Vacuum Ultraviolet Scintillator and Potential Laser Material" (Optical Society of America) Nonlinear Optics Materials, Fundamentals and Applications, junly 30-August 3, 2007 Kona Hawaii, USA, WE29.

8. Marilou M. Cadatal, Young-Seok Seo, Toshihiro Tatsumi, **Minh Hong. Pham**, Carlito Ponseca Jr. Shingo Ono, Elmer Estacio, Yusuke Furukawa, Hidetoshi Murakami, Yasushi Fujimoto, Nobuhiko Sarukura, Masahiro Nakatsuka, Kentaro Fukuda, Rayko Simura, Toshihisa Suyama, Akira Yoshikawa, and T. Fukuda, "Nd^{3+}: $(La_{1-x},Bax)F_{3-x}$ as Vacuum Ultraviolet Scintillator and Potential Laser Material", Conference on Laser and Electro-Optics/Quantum Electronics and Laser Science Conference, May 6011, 2007, Baltimore Convention Center, Maryland, USA, P. JTu A104.
9. Marilou M. Cadatal, **Minh H. Pham**, S. Ono, Elmer Estacio, H. Murakami, Y. Fujimoto, Y. Seo, T. Tatsumi, Nobuhiko Sarukura, M. Nakatsuka, K. Fukuda, Akira Yoshikawa, T.Fukuda, "Comparison of vacuum ultraviolet (VUV) fluorescence from Nd^{3+} - doped LaF_3 and YLiF4" 67^{th} Autumn Meeting of the Japanese Society of Applied Physics, Shiga, Japan, 2006, 30A-ZE-6
10. Marilou M. Cadatal, Young-Seok Seo, Toshihiro Tatsumi, **Minh Hong. Pham**, Carlito Ponseca Jr. Shingo Ono, Elmer Estacio, Yusuke Furukawa, Hidetoshi Murakami, Yasushi Fujimoto, Nobuhiko Sarukura, Masahiro Nakatsuka, Kentaro Fukuda, Rayko Simura, Toshihisa Suyama, Akira Yoshikawa, and T. Fukuda, "Micro-Pulling Down

Grown Nd^{3+}: $(La_{1-x}, Bax)F_{3-x}$ as New Vacuum Ultraviolet Ultraviolet Scintillator and Potential Laser Material", 54 th Spring Meeting of the Japanese Society of Applied Physics, Tokyo, Japan 2007.

11. Marilou M. Cadatal, **Minh Hong. Pham**, Shingo Ono, Carlito Ponseca Jr, Elmer Estacio, Hidetoshi Murakami, Yasushi Fujimoto, Nobuhiko Sarukura, Masahiro Nakatsuka, Kentaro Fukuda, Toshihisa Suyama, Akira Yoshikawa, and T. Fukuda, "Investigation of the Optical Properties of Nd^{3+} - doped LaF_3 and $YLiF_4$ in the Deep Ultraviolet (DUV) and Vacuum Ultraviolet (VUV) Region", The 24th samahang Pisika Pilipinas ng (SPP) Physics Congress, Davao City, Philippines, **3,** 2006, p. spp-2006-008 ISSN 1656-2666.

12. Marilou M. Cadatal, **Minh H. Pham**, Toshihiro Tatsumi, Ayumi Saiki, Yusuke Furukawa, Elmer Estacio, Nobuhiko Sarukura, Toshihisa Suyama, Kentaro Fukuda, Kyoung Jin Kim, and Akira Yoshikawa " All solid state ultraviolet laser from micro-pulling down method grown Ce:LiCAF with direct pumping by the fourth harmonic of a Nd:YAG laser" The 24th samahang Pisika ng Pilipinas (SPP) Physics Congress, Laguna, Philipines, **4,** 2007, p. spp 2007-042, ISSN 1656-2666.